UNITED STATES DEPARTMENT OF THE INTERIOR

GEOLOGICAL SURVEY

Preliminary Results of Deep Electrical Studies in the Long Valley Caldera, Mono and Inyo Counties, California

By

W. D. Stanley, D. B. Jackson, and A. A. R. Zohdy

Open-file report

1973

Illustrations

[Plates are in pocket]

Preliminary results of deep electrical studies in the Long Valley caldera, Mono and Inyo Counties, California

By W. D. Stanley, D. B. Jackson, and A. A. R. Zohdy

Introduction

The U.S. Geological Survey has completed certain phases of extensive geological, geophysical, and hydrological studies in the Long Valley caldera as part of its geothermal research program. This report will provide data and preliminary interpretations from one segment of the geophysical studies, namely deep electrical studies using direct-current and time-domain electromagnetic methods. The goals for the geophysical studies described in this report were (1) to provide additional information on the geology and the structure of the Long Valley caldera, (2) to outline conductivity anomalies caused by thermal effects, and (3) to aid in test hole siting and in evaluation of the overall hydrothermal potential of the caldera system.

The Long Valley area is shown on plate 1. The caldera has been studied by several researchers (Rinehart and Ross, 1964; Pakiser, Kane, and Jackson, 1964; and Bailey, 1973). Bailey's studies are the most detailed and are a major part of the U.S.G.S. geothermal research in the area.

Geophysical techniques

Bipole-dipole mapping techniques (Alpin, 1966; Zohdy, 1973b) were used to compile an apparent resistivity map of the caldera. These data were used to guide the location of electrical and electromagnetic soundings to determine the cause of major electrical anomalies. Forty-nine Schlumberger direct-current soundings (Keller and Frischknecht, 1966) and 13 time-domain electromagnetic soundings (Vanyan, 1966) were completed during the surveys.

The bipole-dipole array used for the studies described in this report is shown in figure 1. A cable approximately 3-5 km long grounded at A and B is excited with a 0.035-0.14 Hz square wave of 10-50 ampere

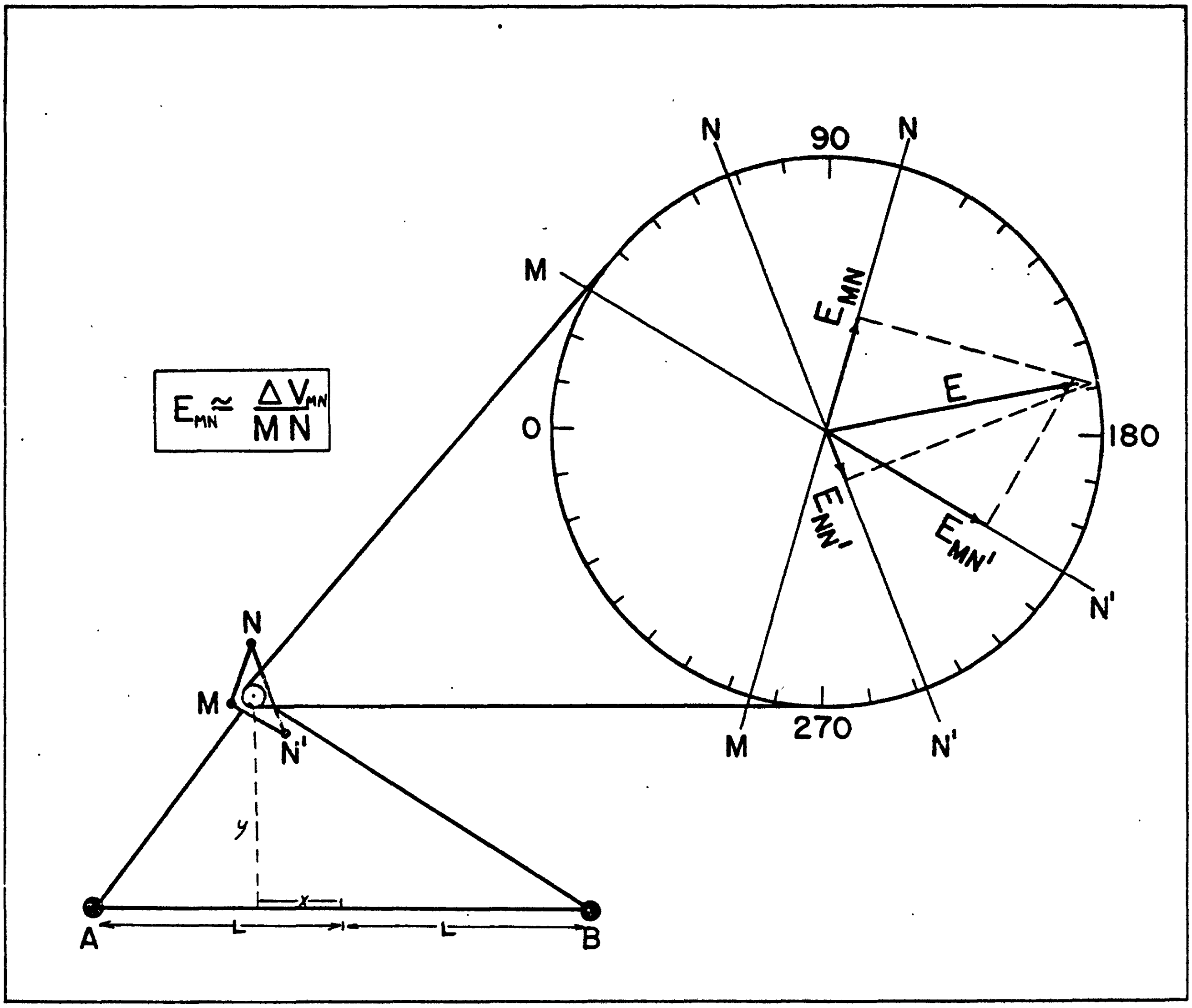

Figure 1.--Bipole-dipole array. A and B are ground electrodes for the bipole transmitter; M, N, and N' are the potential electrodes used to measure the electric field. In the polar plot, E_{MN}, $E_{MN'}$, and $E_{NN'}$ are the measured electric fields and E the maximum field resolved from these components.

peak amplitude. The resulting electric field at a field station is measured using the array MN-MN'. The polar plot in the upper right portion of the figure illustrates the procedure for determining the total electric field, E. The apparent resistivity (or simple total field resistivity, Zohdy, 1973b) is determined from the equation:

$$\bar{\rho}_E = K_{e_o} \frac{|E|}{I}$$

where $|E|$ is the measured total electric field, regardless of direction, I is the input current, and K_{e_o} is the geometric factor defined by:

$$K_{e_0} = \frac{\rho_0}{E_0} = \frac{2\pi}{\left\{\left(\frac{y}{AO^3}-\frac{y}{BO^3}\right)^2+\left(\frac{x+L}{AO^3}-\frac{x-L}{BO^3}\right)^2\right\}^{\frac{1}{2}}}$$

where E_o is the electric field magnitude which would be measured over a homogeneous half-space of resistivity ρ_o with an input current of I, and x, y, L, AO, and BO are as indicated in figure 1. A calculator which can be programmed is used to reduce the field data, i.e., to resolve the measured electric field components into the total field, to compute a geometric factor, and finally to compute the apparent resistivity for the field station.

Direct current soundings were made using the Schlumberger array (Keller and Frischknecht, 1966); apparent resistivities for the Schlumberger array, $\bar{\rho}_s$ are computed from:

$$\bar{\rho}_s = \pi \left[\frac{(AB/2)^2}{MN} - \frac{MN}{4}\right] \left[\frac{V_{mn}}{I}\right]$$

where AB and MN are the current electrode and potential electrode spacings, respectively. V_{mn} is the potential difference between M and N, and I is the input current. Potentials for the Schlumberger soundings and for the bipole-dipole electric field mapping were measured using strip chart recorders.

The time-domain electromagnetic soundings were made by measuring the transient vertical magnetic field, H_z, caused by the current transition at the square wave input to the grounded wire. A complete solution for the time-domain vertical magnetic field over a horizontally layered earth has been developed by Anderson (1973). Additional programs recently developed by Anderson (written commun., 1973) allow consideration of the wire length. These programs were used to compute theoretical curves for trial earth models to fit the field data. Measurements of dB_z/dt were made with a large air-core loop of effective area of 256,000 m^2 turns. Recordings were made of the loop output voltage on a galvanometer type strip-chart recorder with high-gain preamp. The recorder has a response of 70 Hz for 50 percent full-scale deflection. The only filtering incorporated was a high Q notch filter for 60 Hz rejection. Shown in figure 2 are the recording system step response and a typical field recording. Rise time of the input current waveform was less than one millisecond for the worst case of grounding conditions in these surveys.

Interpretations

Three hundred sixty-five electric field measurements were made using four separate bipoles in compiling a resistivity map of the Long Valley caldera. Many of the measurement stations were reoccupied from more than one transmitter location. Four separate apparent resistivity maps were compiled from the field data. In order to compare the resistivity data with the geology and to obtain an overall electrical view of the caldera, the maps from bipoles 2, 3, and 4 were combined into one map as shown in plate 2. Complete maps from bipoles 2, 3, and 4 are represented in plate 2. As seen, the major process in this synthesis of the composite map involved substituting bipole-2 data for about half of the bipole-3 data. It is obvious that the electrical low near bipole 3 shows up very clearly from bipole 2. We chose bipole-2 data because, in general, the greater separation between transmitter and receiver means that the effective probing depths (Keller, 1966) are greater. Other schemes of combining bipole-dipole resistivity maps have been investigated, but for this report we chose this most straightforward method.

Bipole-1 (pl. 3) data overlap the data of bipole 2. We have found from sounding interpretations that the bipole-2 data give a more accurate representation of the subsurface electrical units. In addition, we achieved much more extensive coverage from bipole 2. For these reasons bipole-2 data were used in the composite resistivity map.

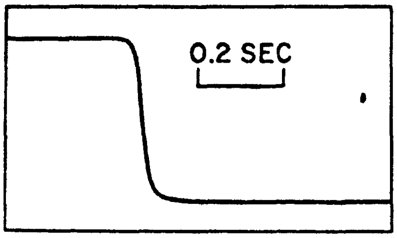

RECORDING SYSTEM STEP RESPONSE

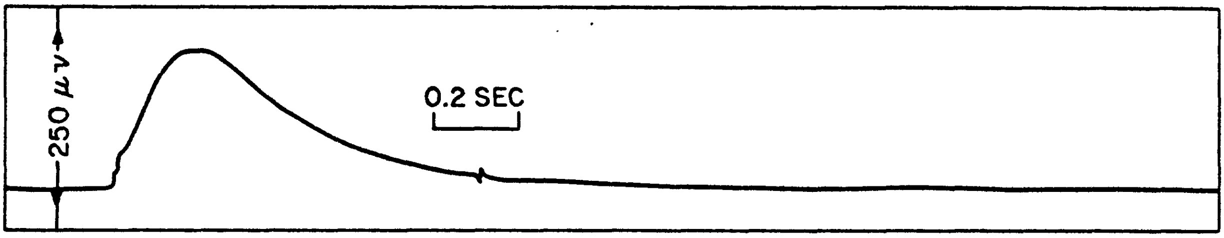

TYPICAL FIELD RECORDING

Figure 2.--A field recording of the transient magnetic field (lower) and the TMS receiver step response (upper).

The composite resistivity map, thermal activity, and faulting are shown on plate 4. One of the major electrical anomalies seen on this map is the large low centered near Cashbaugh Ranch. Notice that this low extends southward intersecting the Hilton Creek fault. The extension of the low in this general direction suggests that either alteration along the fault or inflow of thermal waters along the fault has lowered resistivities in this area.

The Hilton Creek fault appears to splinter into a splayed fault set where the fault makes the transition from the Sierran block to the eastern caldera block. Most of the hot springs on the east side of the resurgent dome (Bailey, 1973) probably owe their location to the existence of this splayed fault set. Recent hot-spring development (in August and October 1973) is confined to the north end of a small graben outlined by an area of less than 10 ohm-meters SW of Cashbaugh Ranch on the resistivity map. The springs broke out near the water surface in Hot Creek downstream from an area of active hot springs used as a bathing area in sec. 30, T. 3 S., R. 28 E., after earthquakes south and southeast of the caldera (D. G. Hill, oral commun., 1973).

Referring to the geologic map (pl. 5), it can be seen that the Cashbaugh resistivity low extends northwest into an area of outcrops of a dome-tuff unit, suggesting that the tuff unit may be the cause of part of the low. Evidence from soundings and from a recent drill hole also suggest that this tuff unit is the conductor observed in the Cashbaugh low.

In addition to the Cashbaugh low there is an L-shaped low in the Casa Diablo area (pl. 4). Referring to the aeromagnetic map (Pakiser and others, 1964) in plate 6, we see that there is a coincident magnetic field low. Sounding data show that this electrical low is caused by a conductive layer or zone at a depth of about 30-200 m. The anomaly is apparently fault controlled and probably represents extensive past hydrothermal alteration, the low resistivities being mainly due to high clay content and the low susceptibilities due to destruction of magnetite by hot waters.

Shown on both the electrical and aeromagnetic maps (pls. 4 and 6) is a set of apparent structural trends. The NW trend is quite evident on both maps and probably represents major regional control of events within the caldera. Notice that if this trend is projected outside the caldera, it lines up with the Hilton Creek fault to the southeast. For the most part these trends define the boundary of the resurgent dome described by Bailey (1973). The caldera portion east of the northwest trend appears to have behaved as a separate unit. This trend also is illustrated on plate 7 by the gravity data (from Pakiser and others, 1964). The major aeromagnetic high which lies along the northeast edge of this trend probably is caused by magnetite-rich flows associated with this structural feature. The extension of this high to the eastern part of the caldera probably represents large lateral flows from sources near the structural zone.

Sounding interpretations

Forty-nine vertical electrical soundings (VES) using the Schlumberger array were completed in the caldera with maximum electrode spacings, AB/2, ranging generally from 1.22 to 3.66 kilometers. Field curves for all of these soundings are shown in figures 3-51. Thirteen transient electromagnetic soundings (TMS) were completed using bipoles 1 and 2. Most of the VES curves were interpreted using an automatic interpretation program developed by Zohdy (1973a). The detailed solutions from this program were simplified using Dar Zarrouk curves (Zohdy, in press) to provide reasonable geologic models. The TMS data were used to help determine true resistivities of conductors observed on VES curves, but whose resistivities could not be determined accurately (on curves with H-type final portions) and to map parameters of conductors beyond the capability of the VES soundings with the electrode spacings used.

Two cross-sections were constructed from the VES and TMS interpretations. The location of profiles A-A' and B-B' are shown on plate 8. The locations of all VES and TMS stations are shown on plate 14. Geoelectrical cross-section A-A' and a profile of total-field apparent resistivities are shown on plate 9. Of most interest in this cross-section is the 1 to 4.5 ohm-meter layer which occurs on the western half of the profile. Drilling data from test hole LV1 indicate that the conductive materials are highly altered tuffs and ash beds with bottom-hole temperatures of about 75°C. (R. E. Lewis, oral commun.,

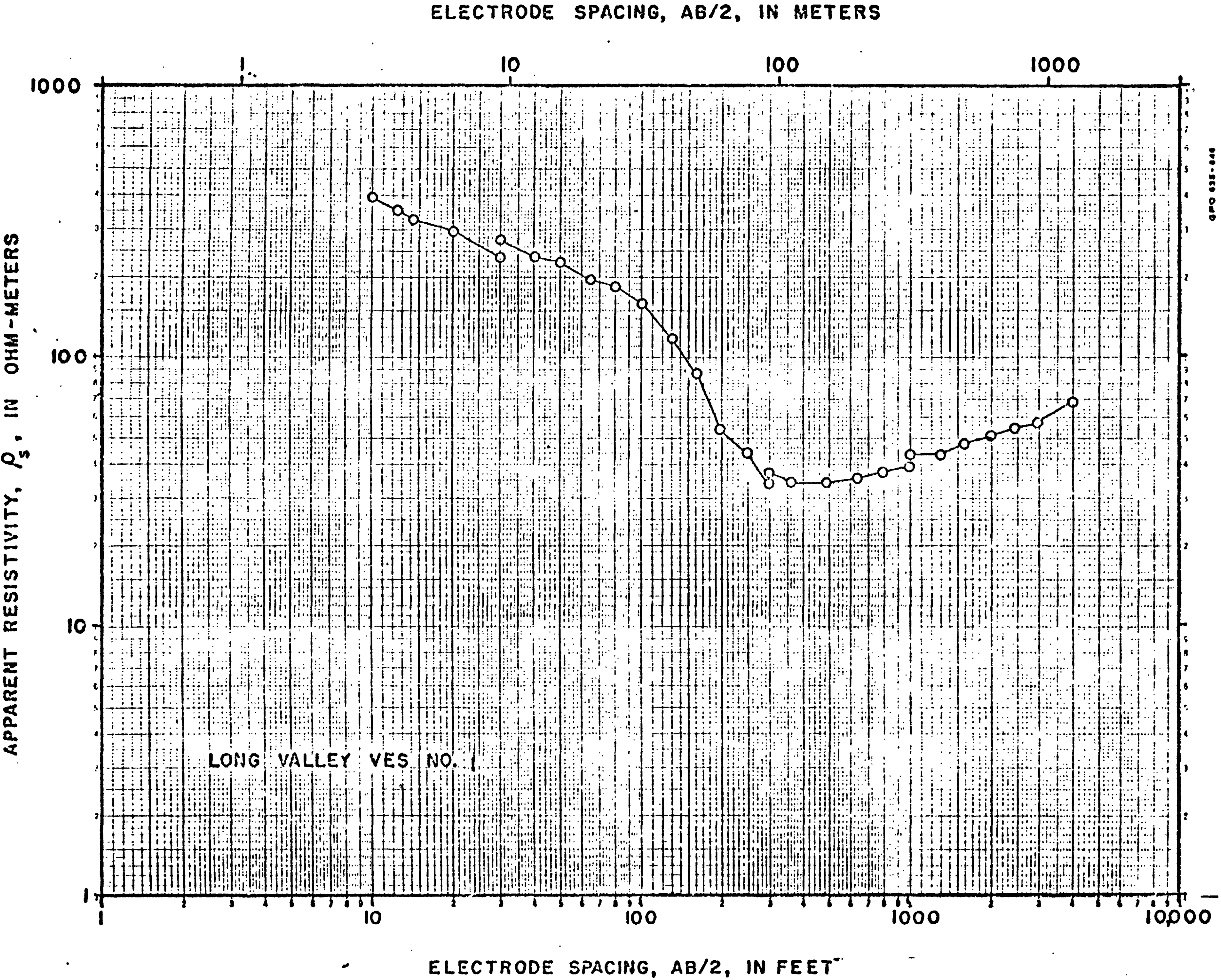

Figure 3.--Schlumberger sounding curve VES 1.

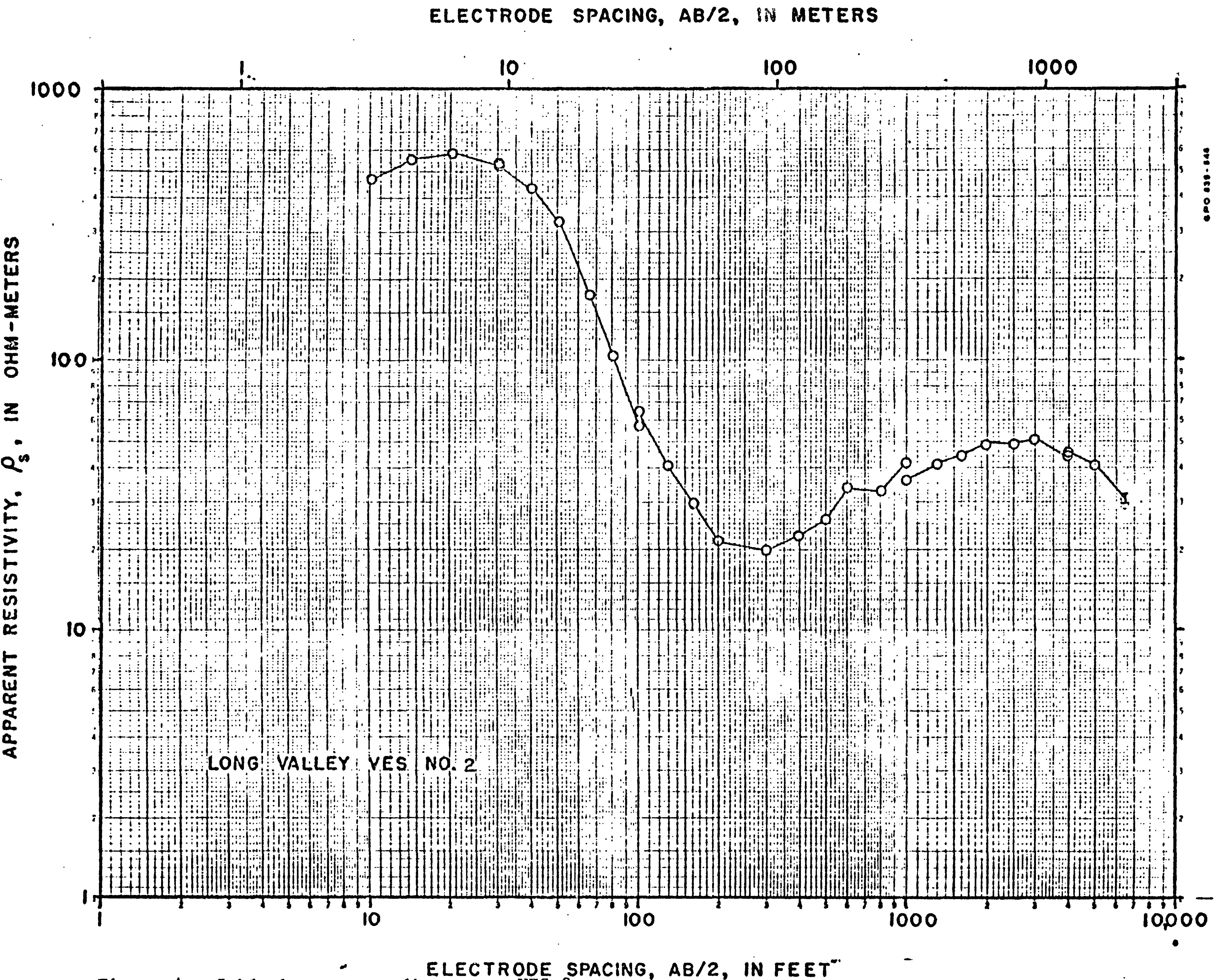

Figure 4.--Schlumberger sounding curve VES 2.

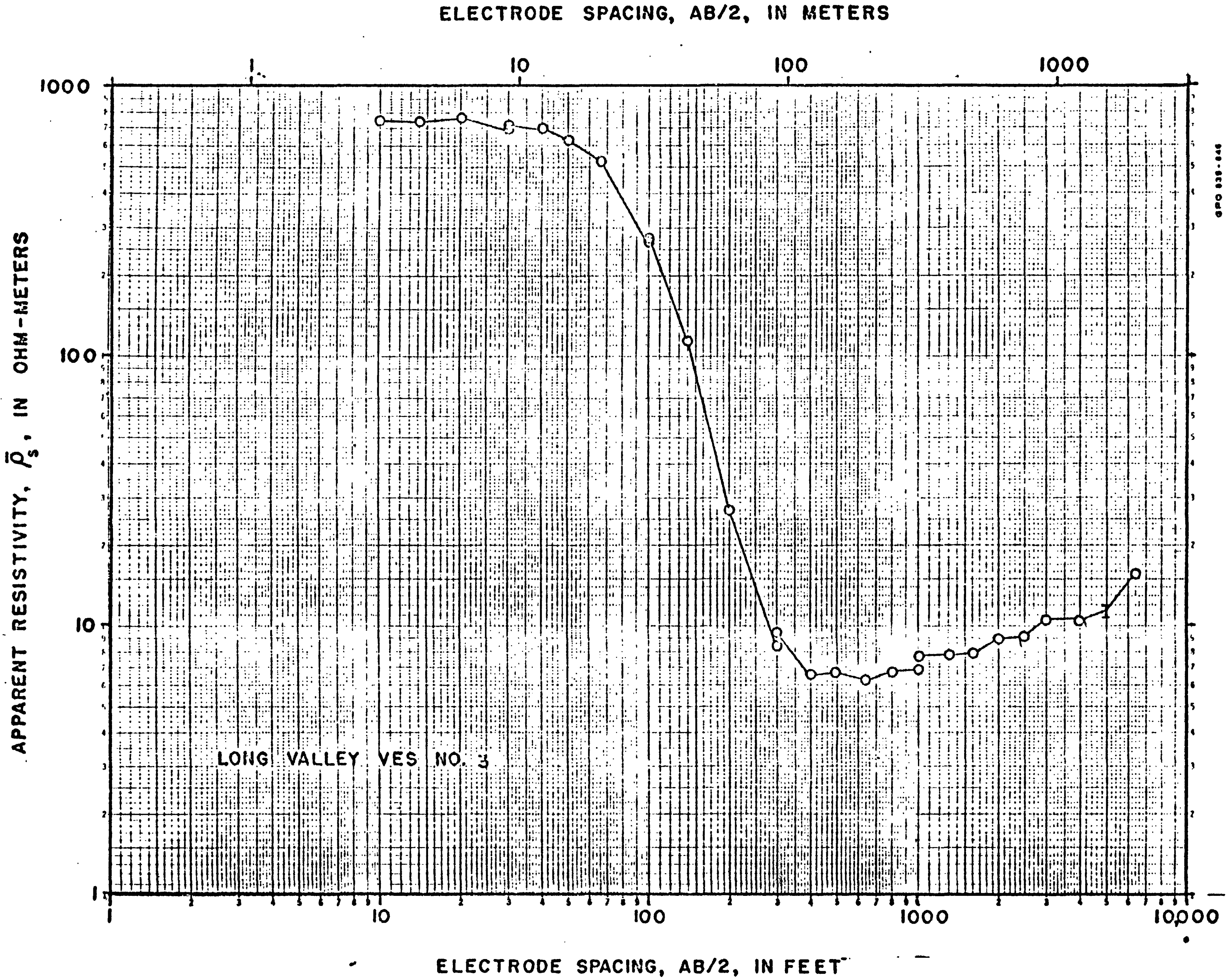

Figure 5.--Schlumberger sounding curve VES 3.

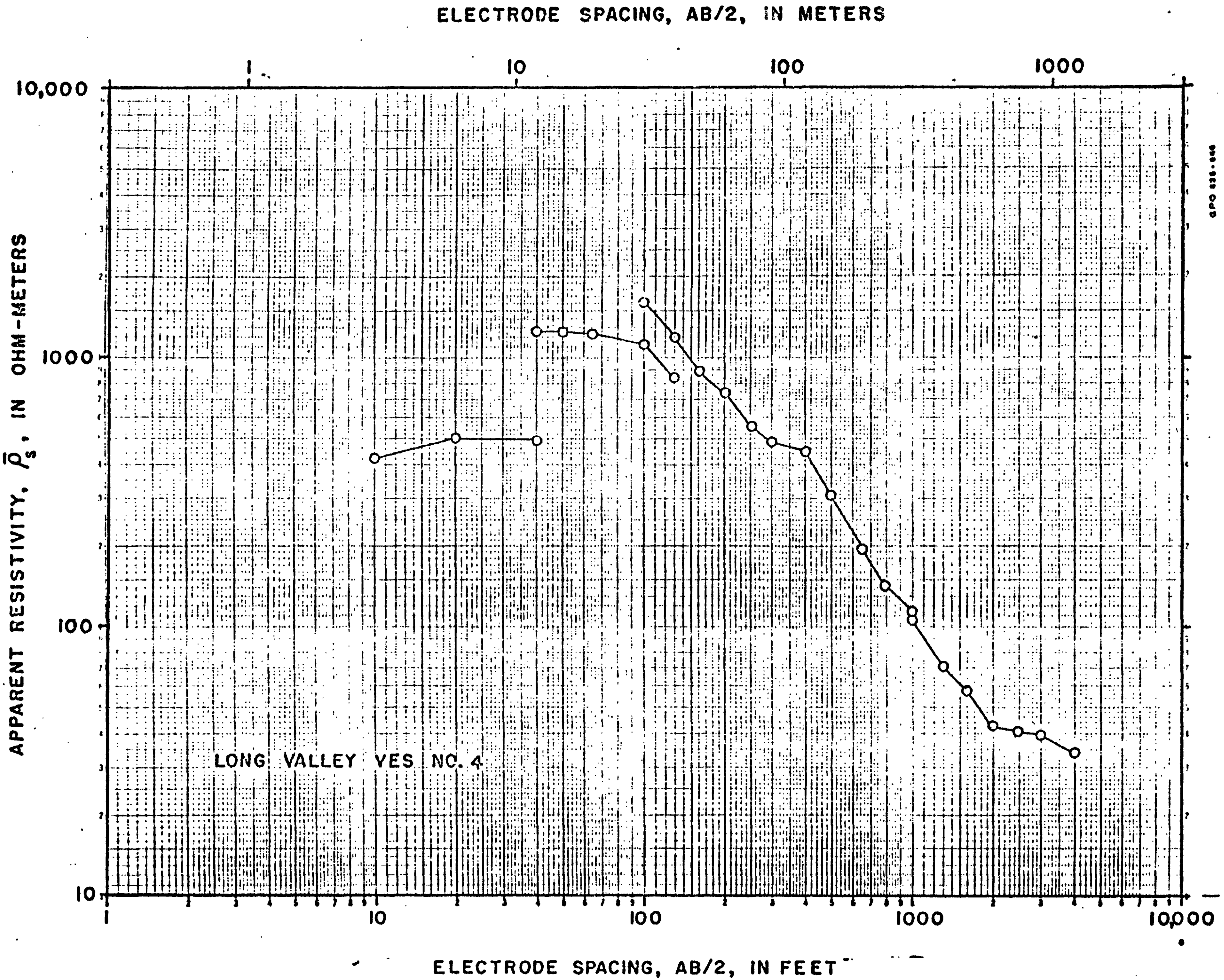

Figure 6.--Schlumberger sounding curve VES 4.

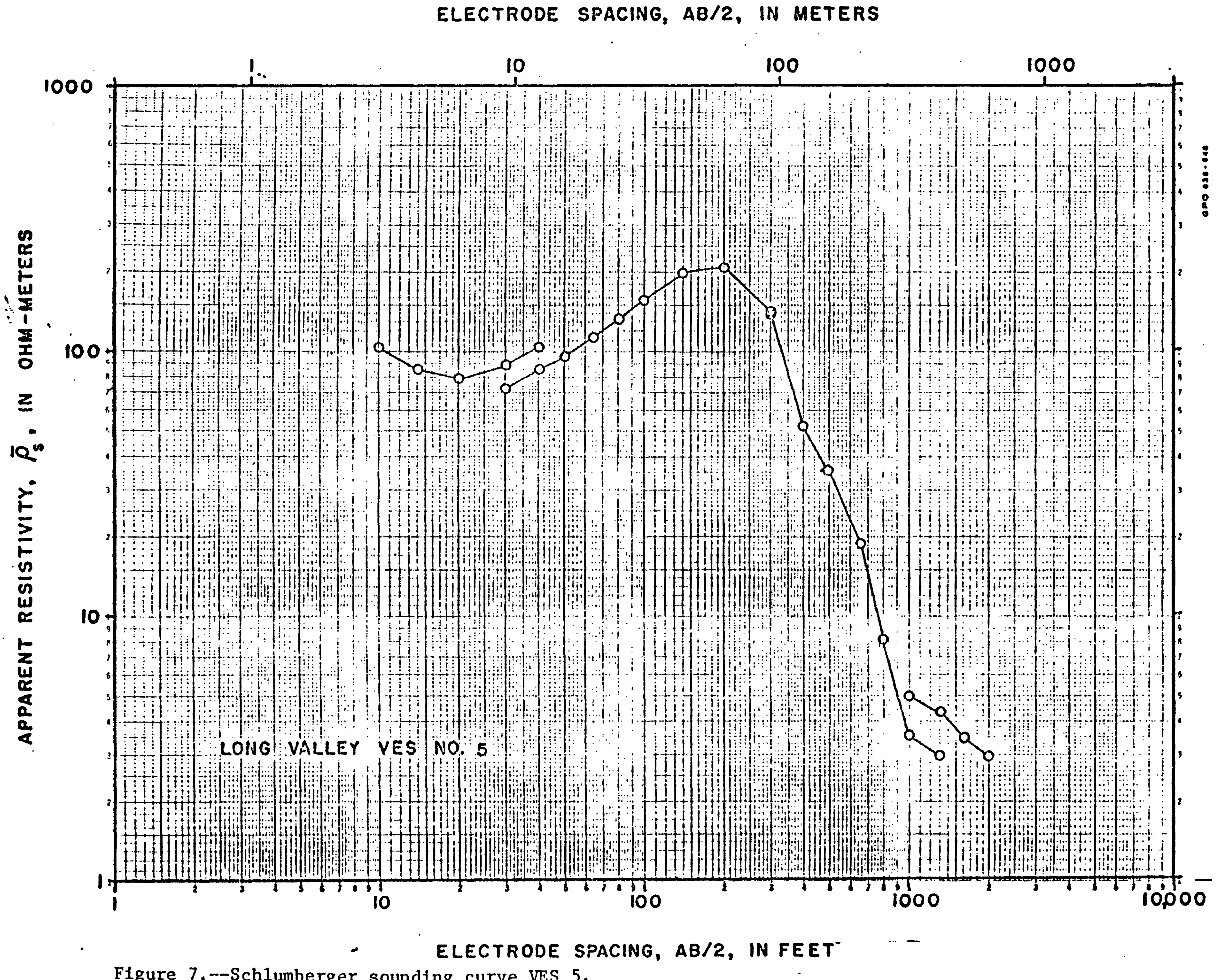

Figure 7.--Schlumberger sounding curve VES 5.

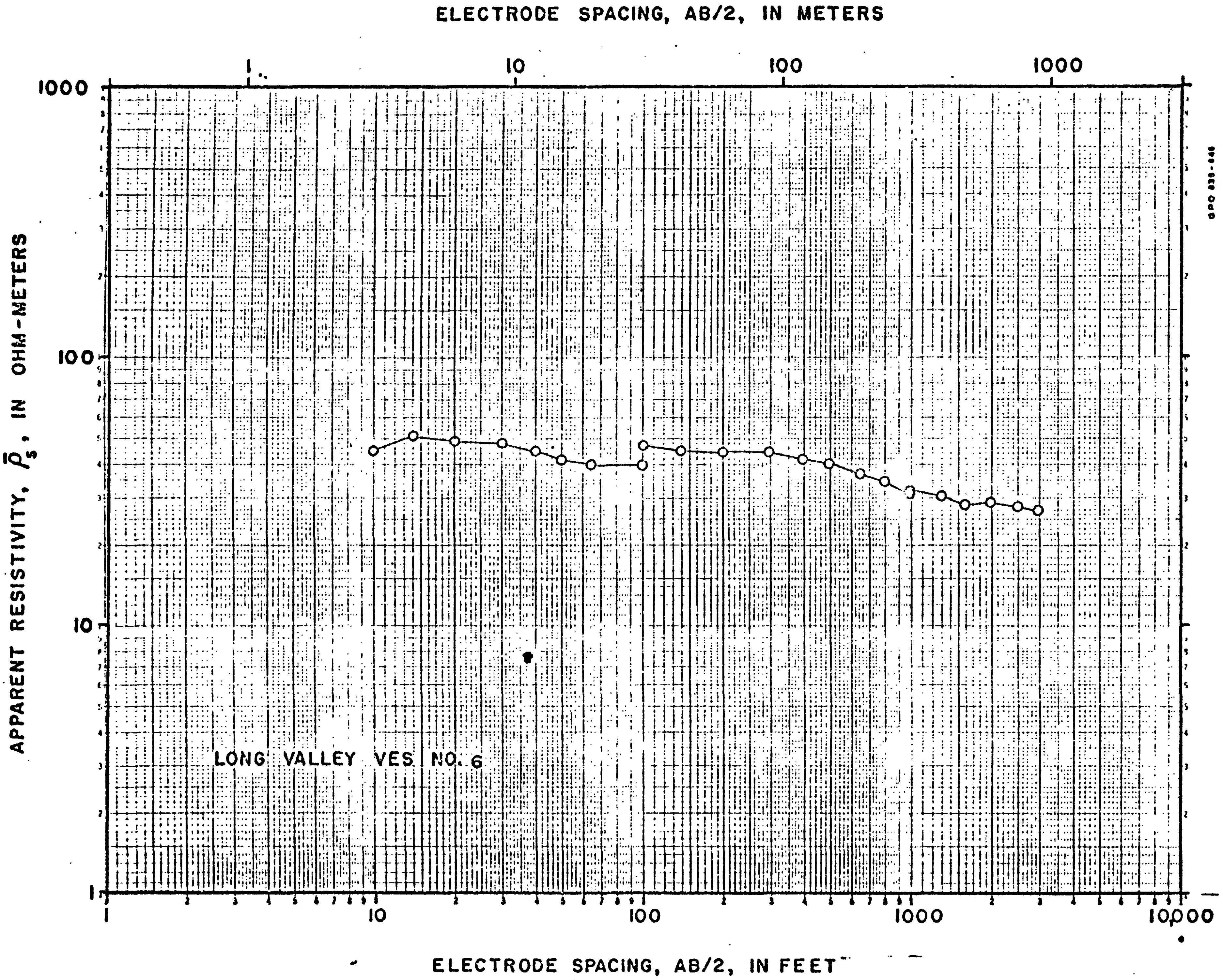

Figure 8.--Schlumberger sounding curve VES 6.

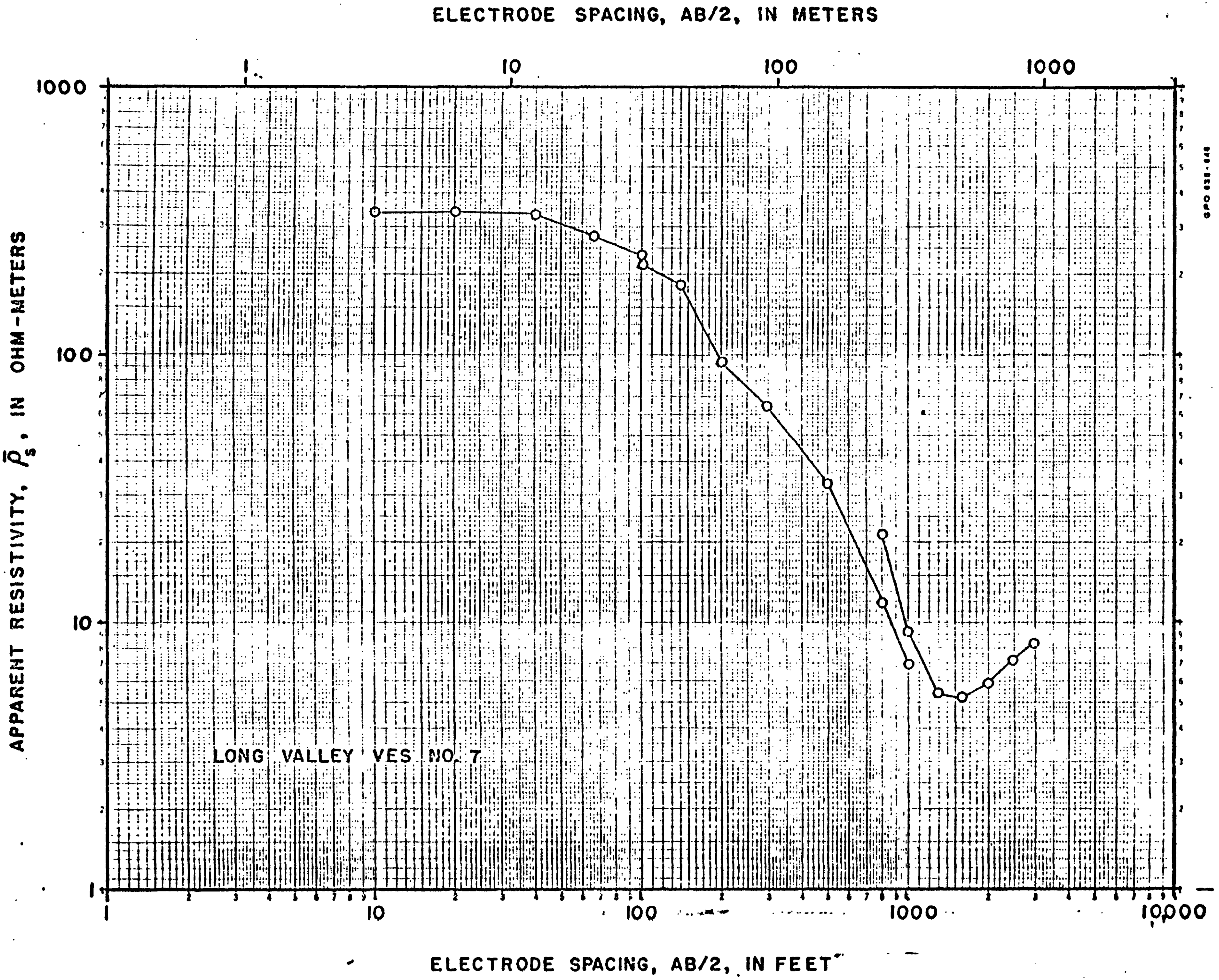

Figure 9.--Schlumberger sounding curve VES 7.

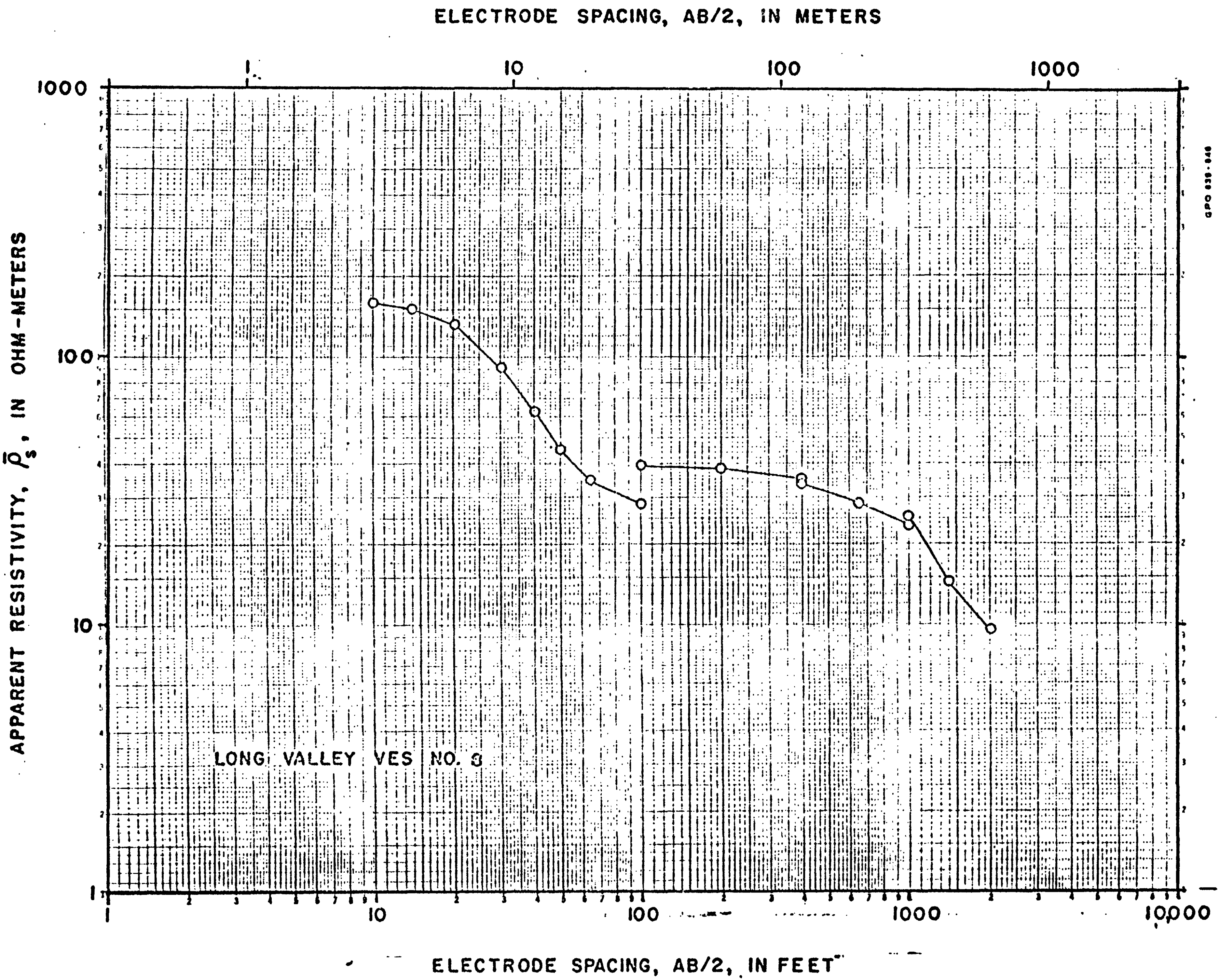

Figure 10.--Schlumberger sounding curve VES 8.

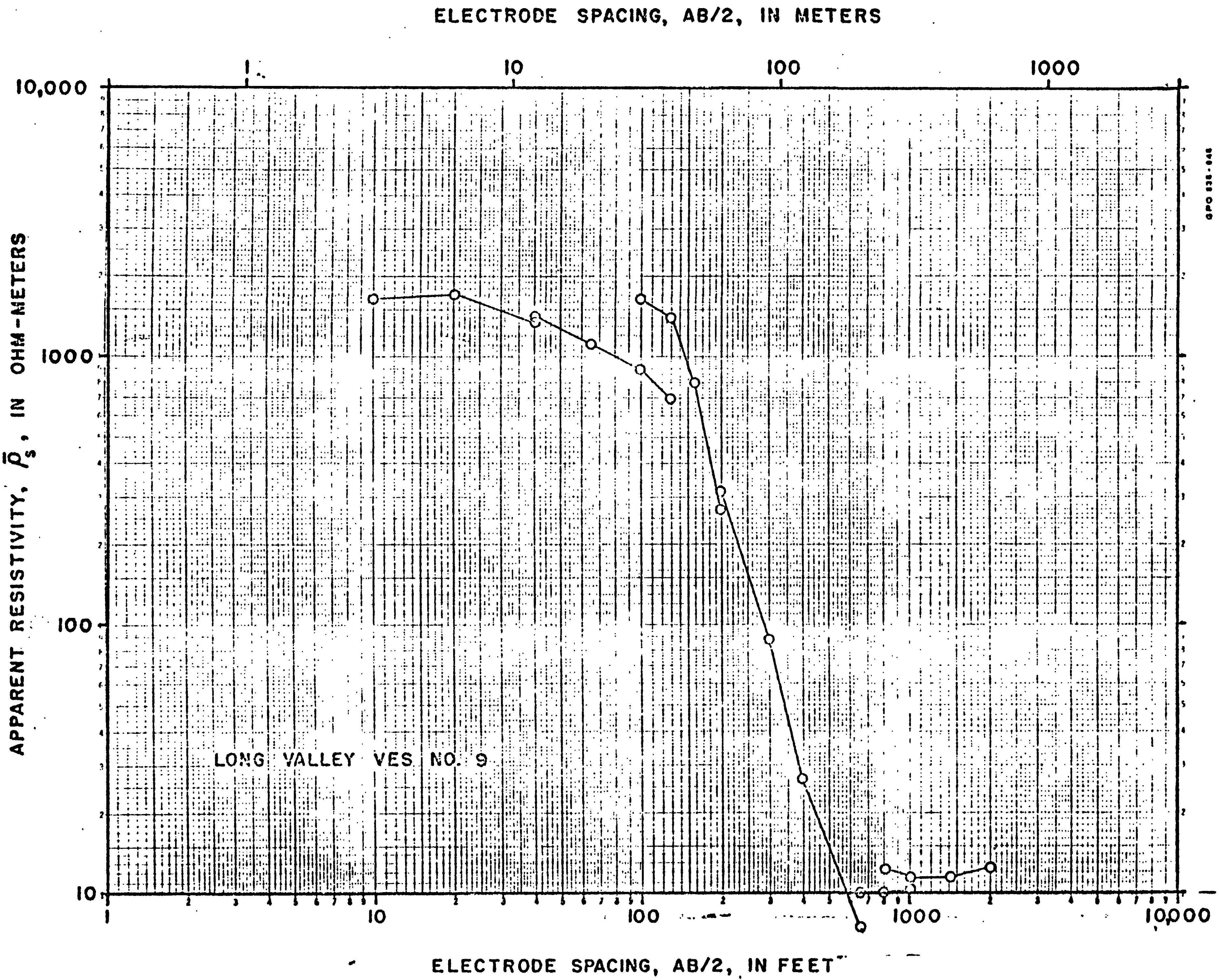

Figure 11.--Schlumberger sounding curve VES 9.

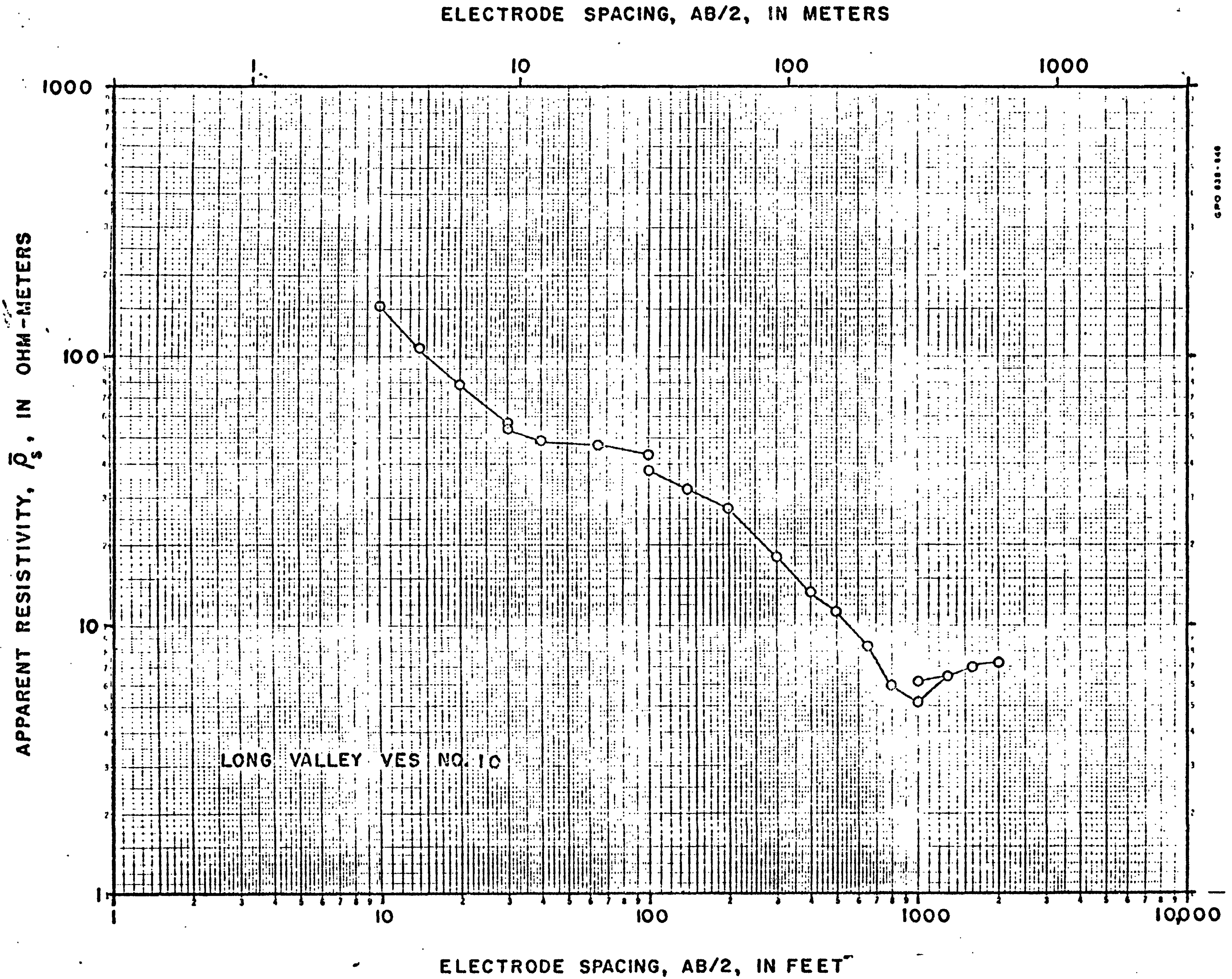

Figure 12.--Schlumberger sounding curve VES 10.

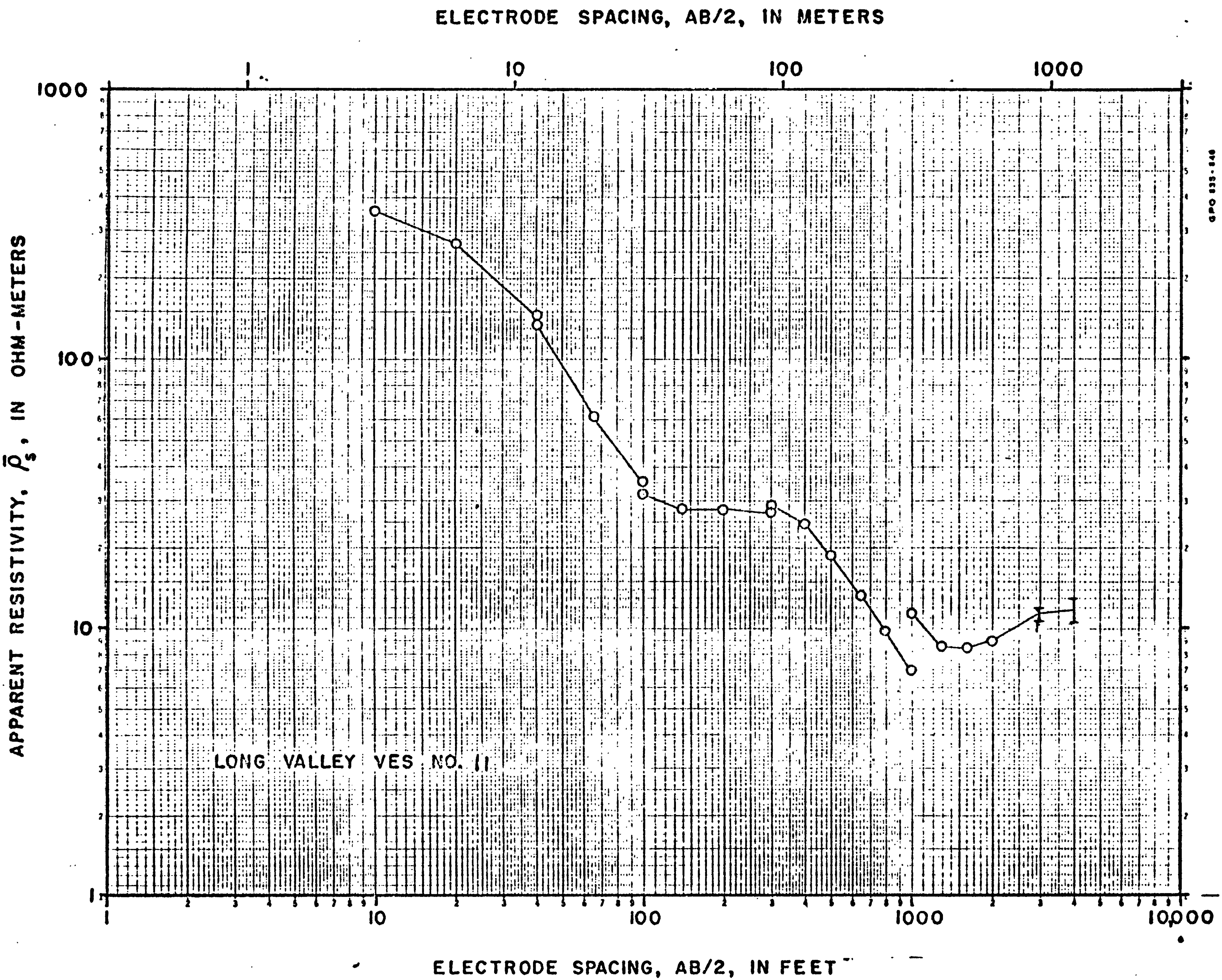

Figure 13.--Schlumberger sounding curve VES 11.

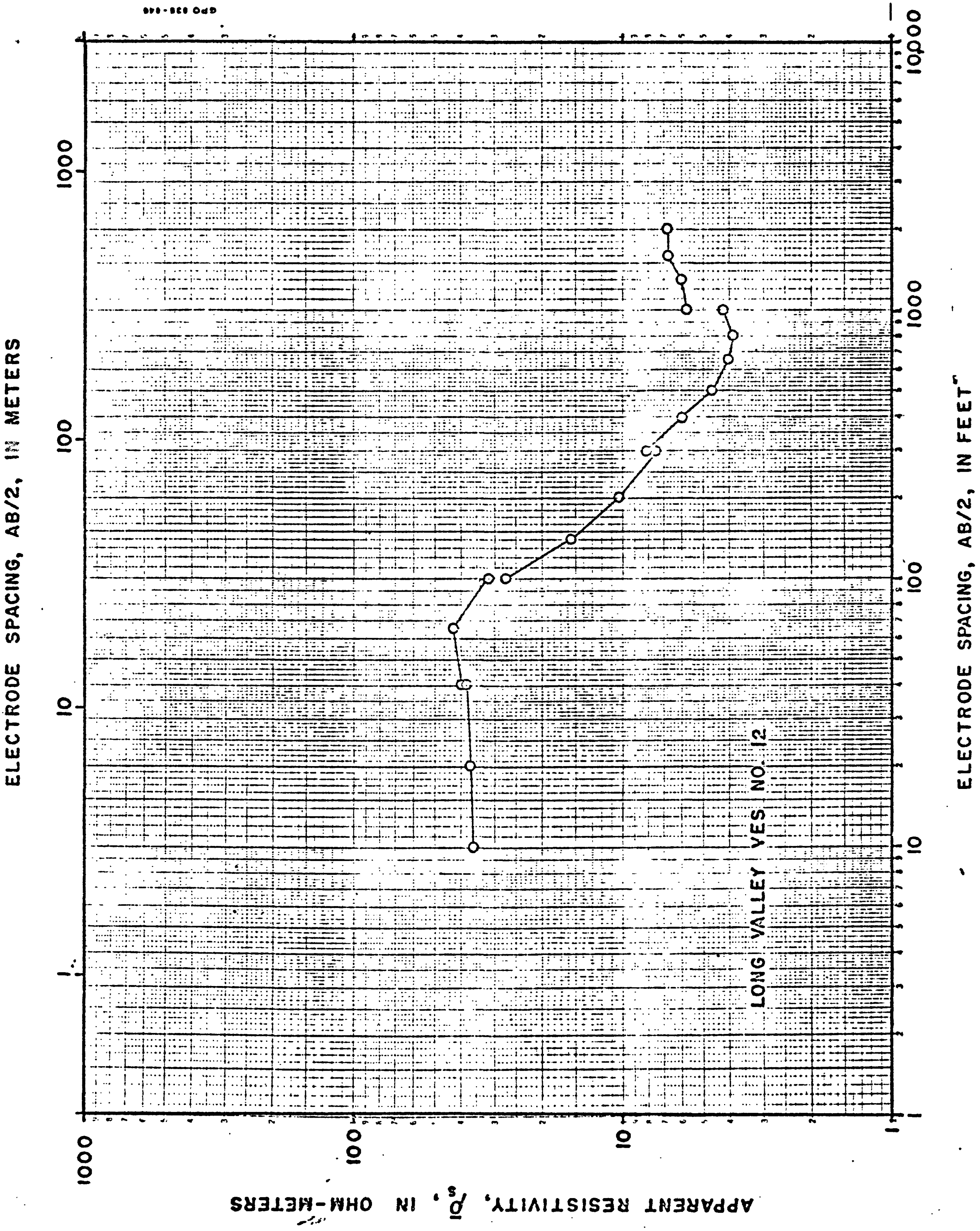

Figure 14.--Schlumberger sounding curve VES 12.

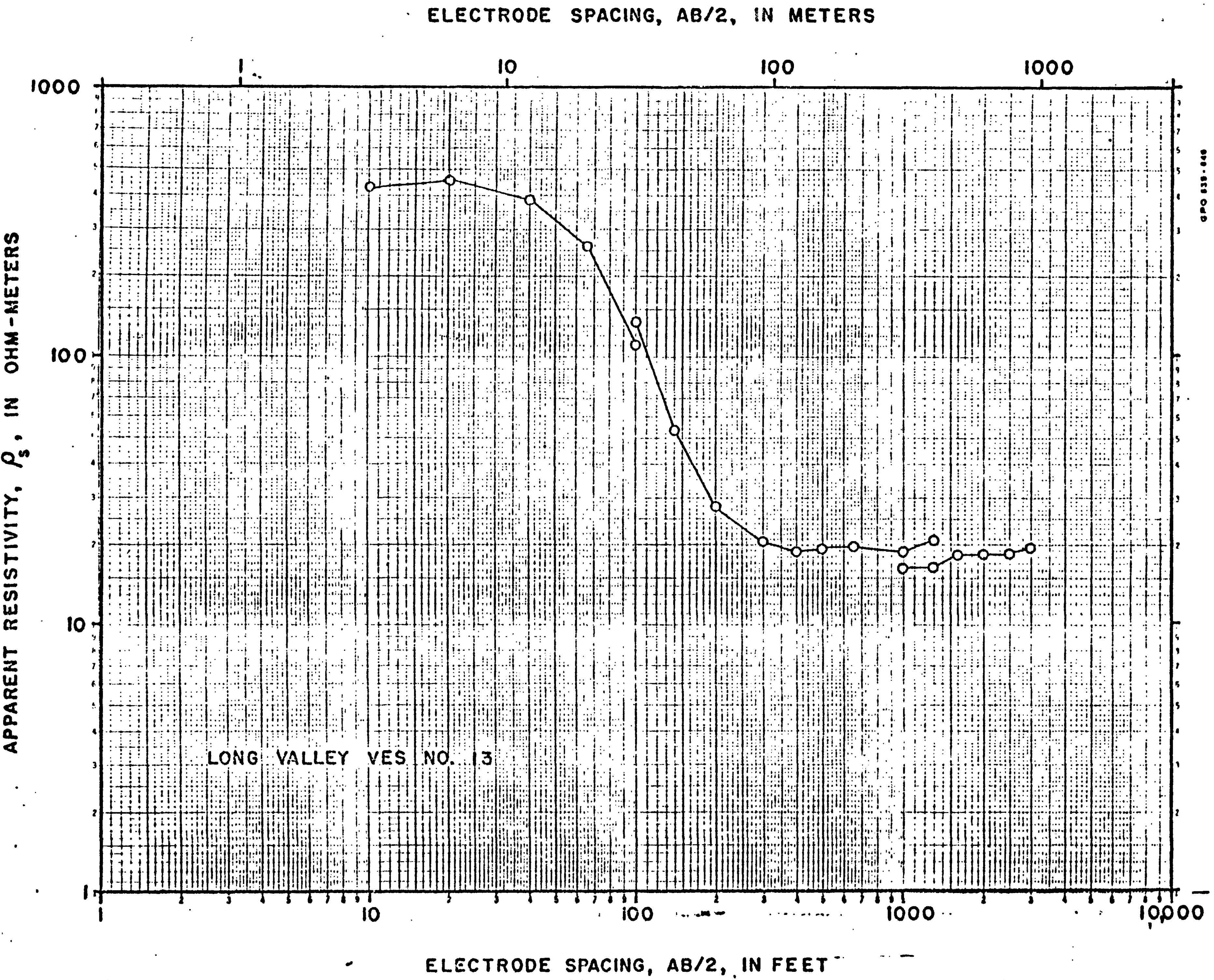

Figure 15.--Schlumberger sounding curve VES 13.

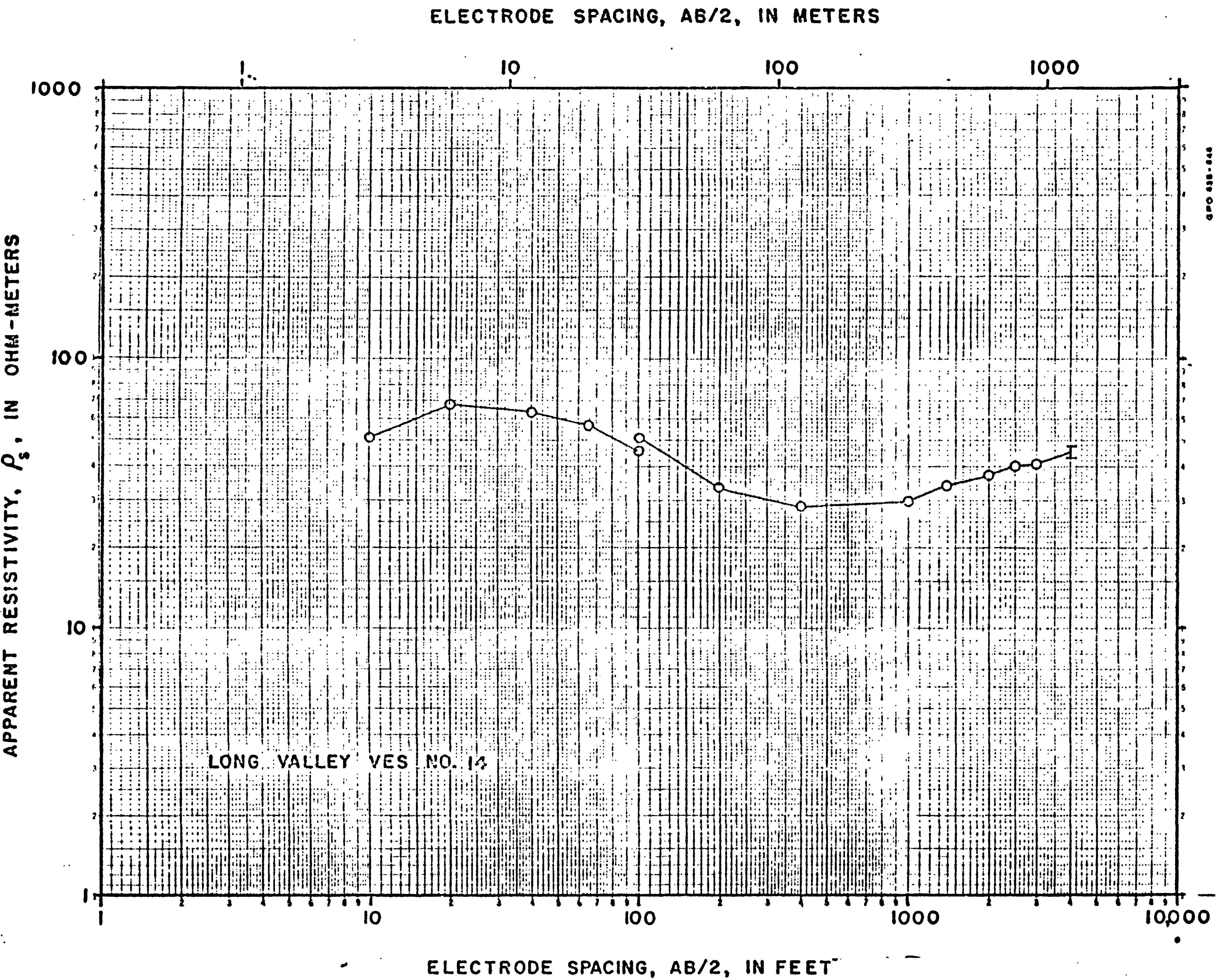

Figure 16.--Schlumberger sounding curve VES 14.

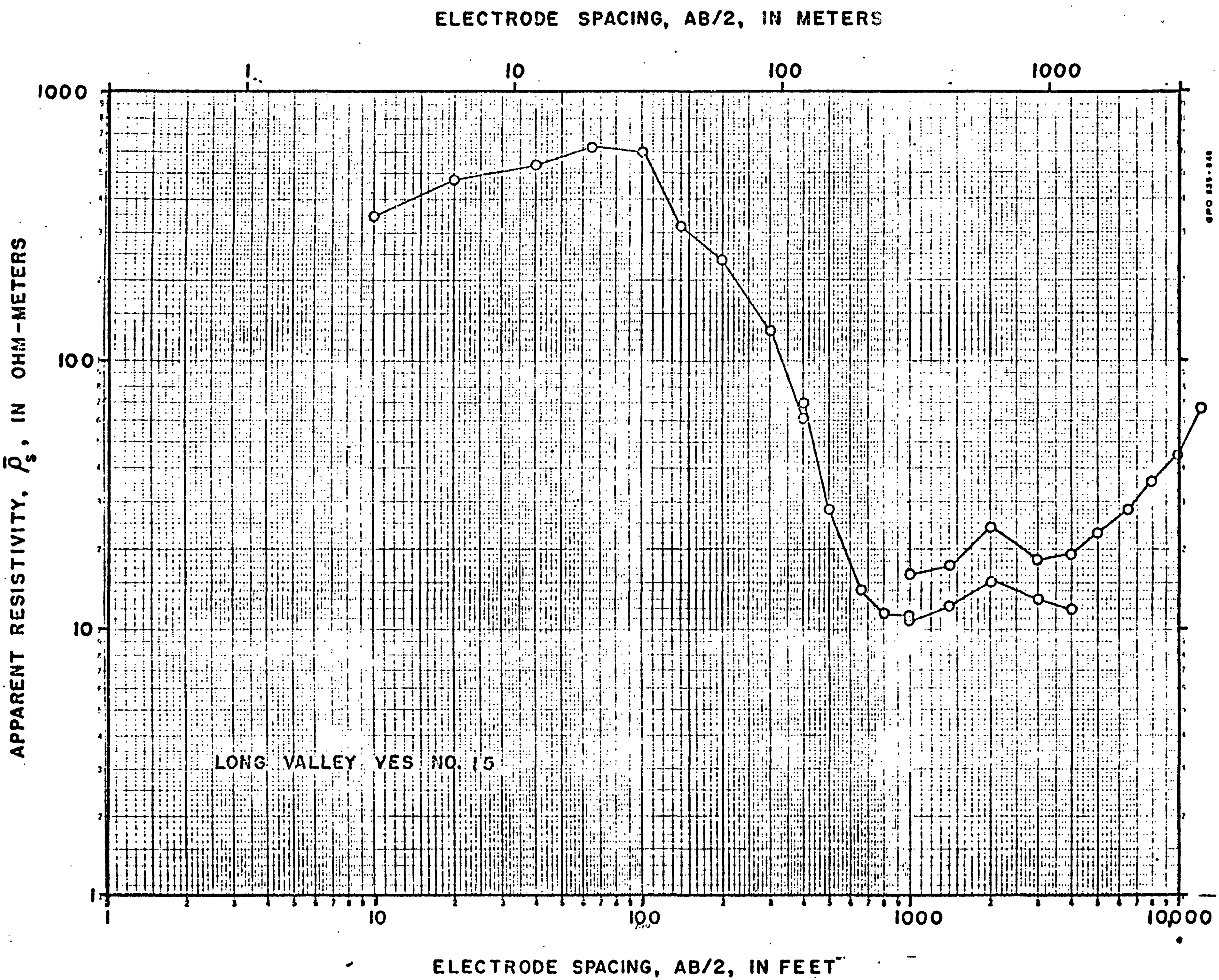

Figure 17.--Schlumberger sounding curve VES 15.

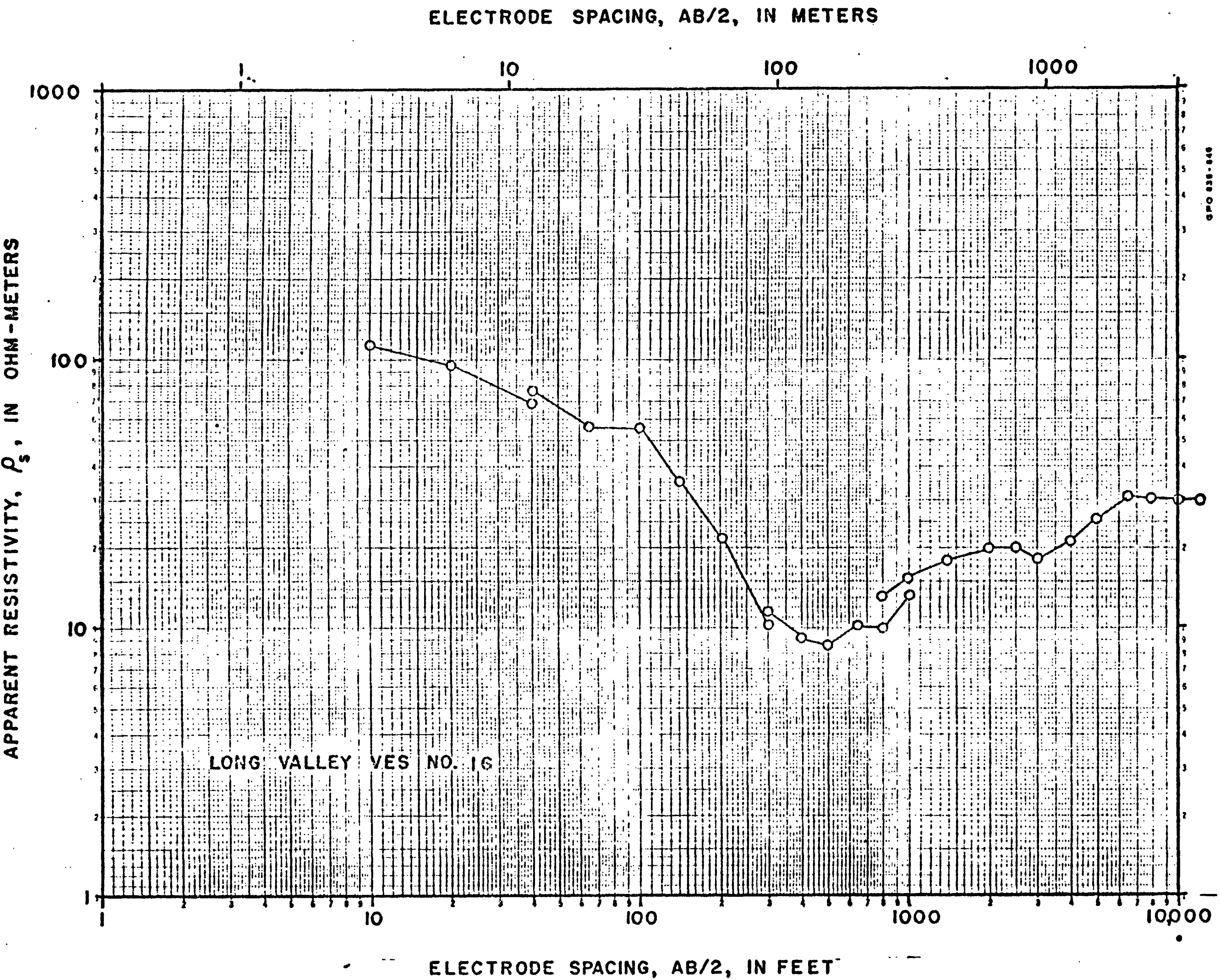

Figure 18.--Schlumberger sounding curve VES 16.

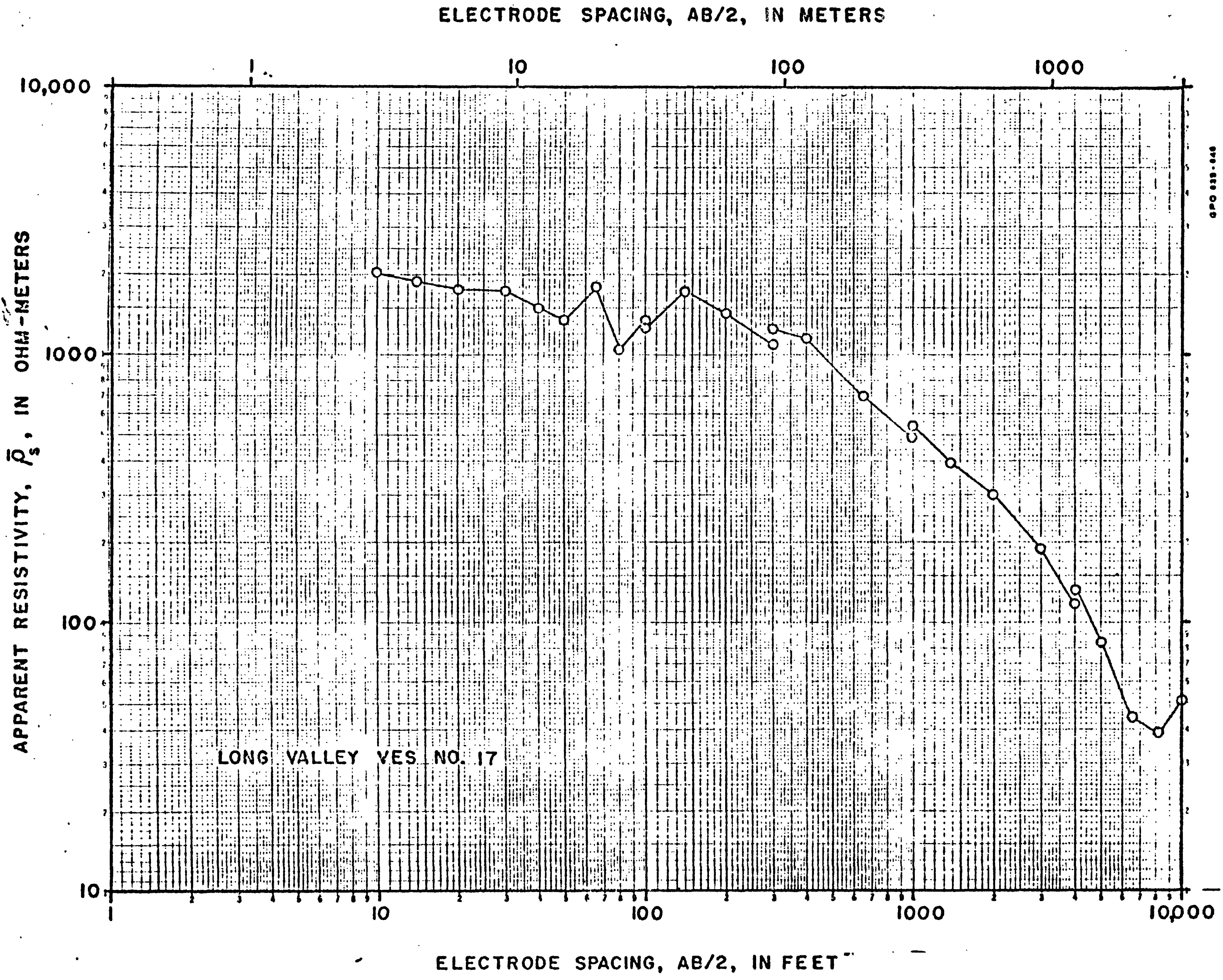

Figure 19.--Schlumberger sounding curve VES 17.

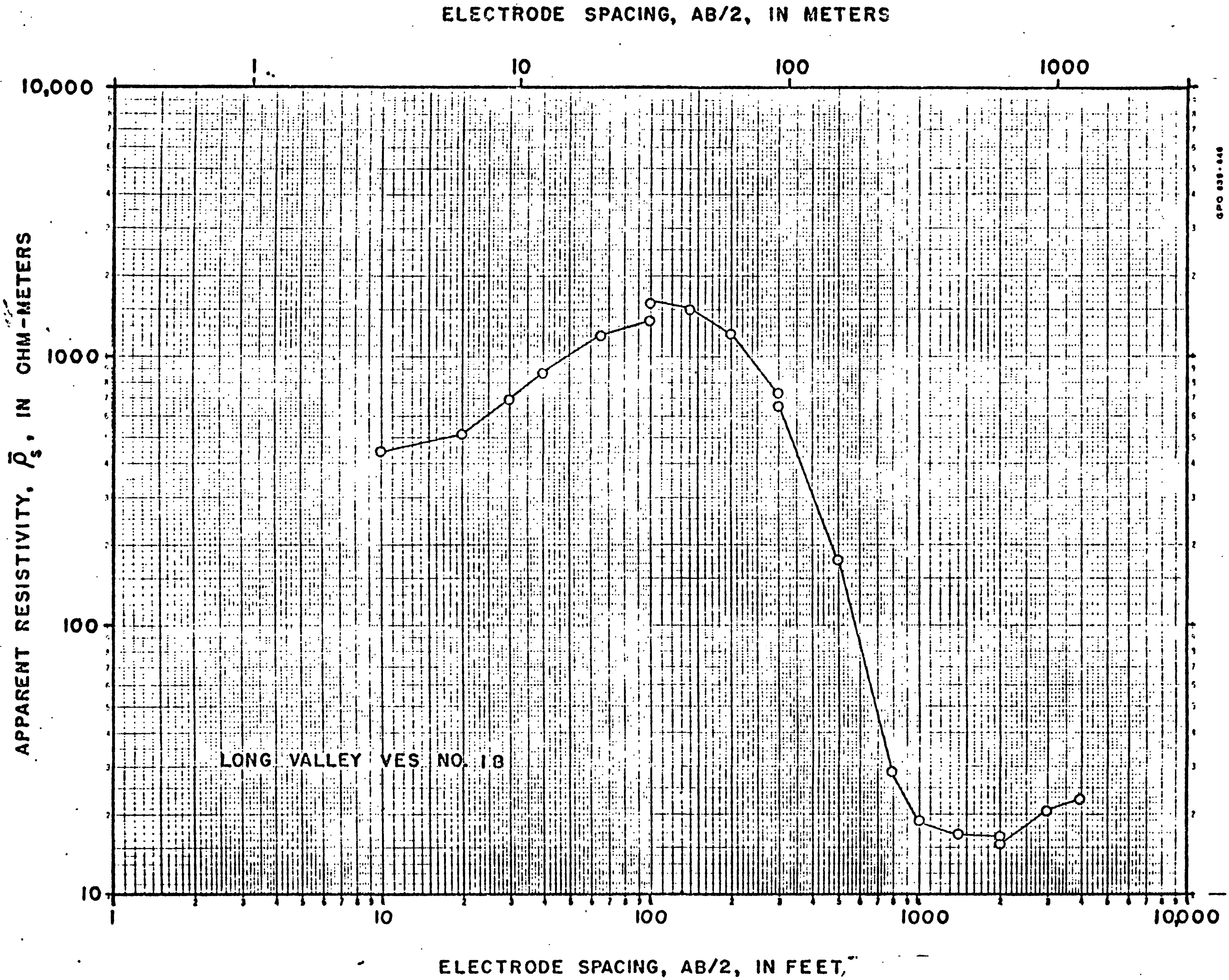

Figure 20.--Schlumberger sounding curve VES 18.

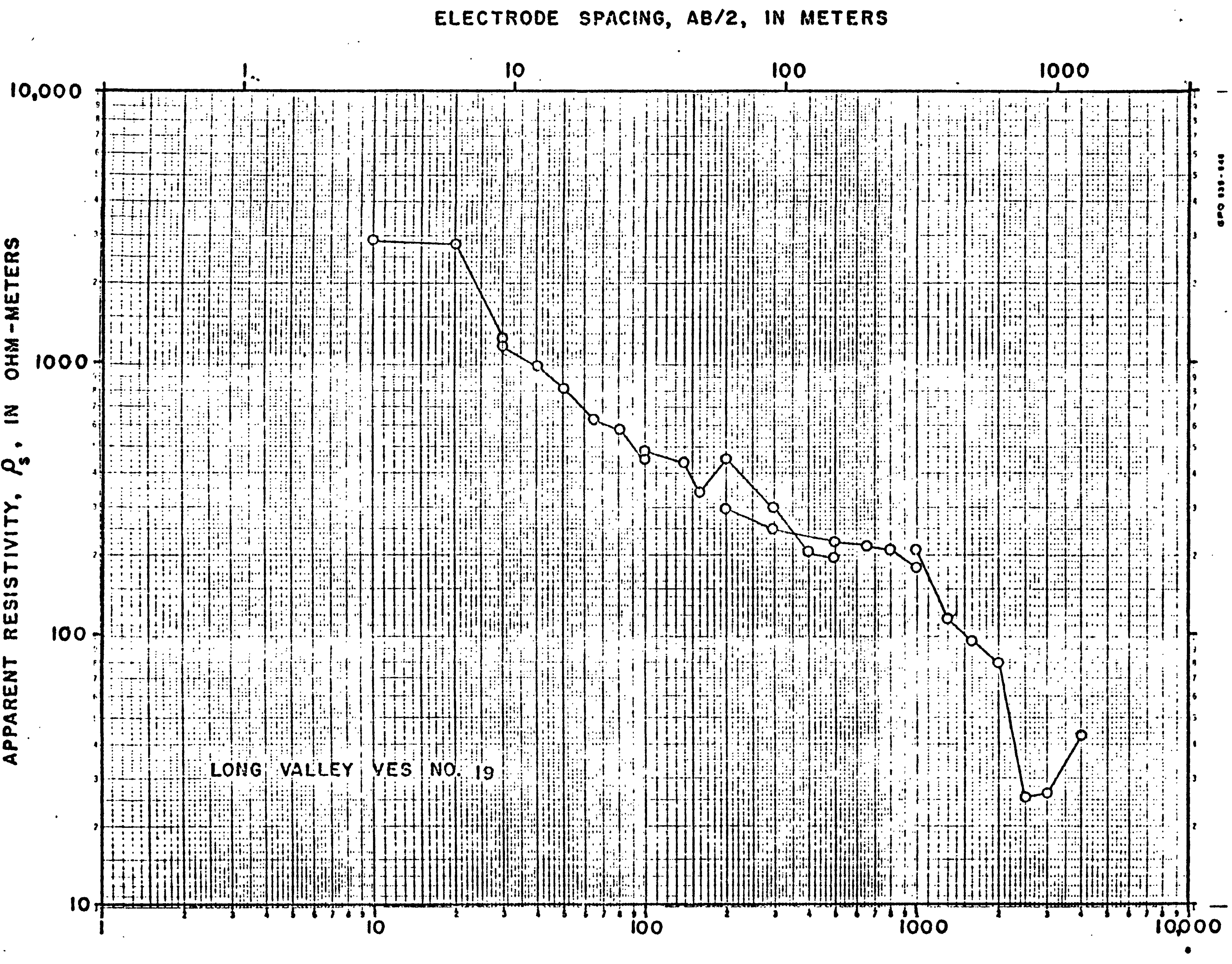

Figure 21.--Schlumberger sounding curve VES 19.

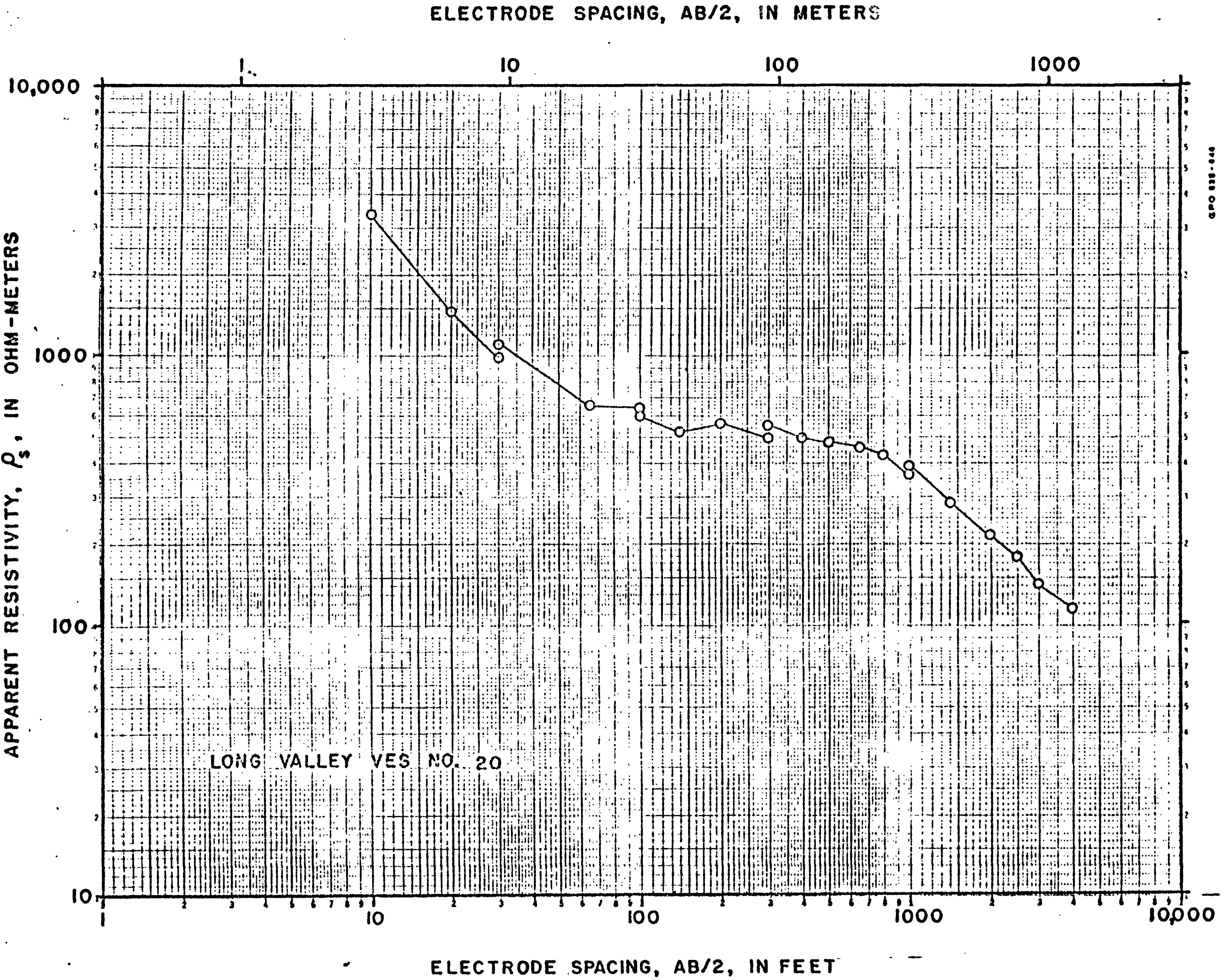

Figure 22.--Schlumberger sounding curve VES 20.

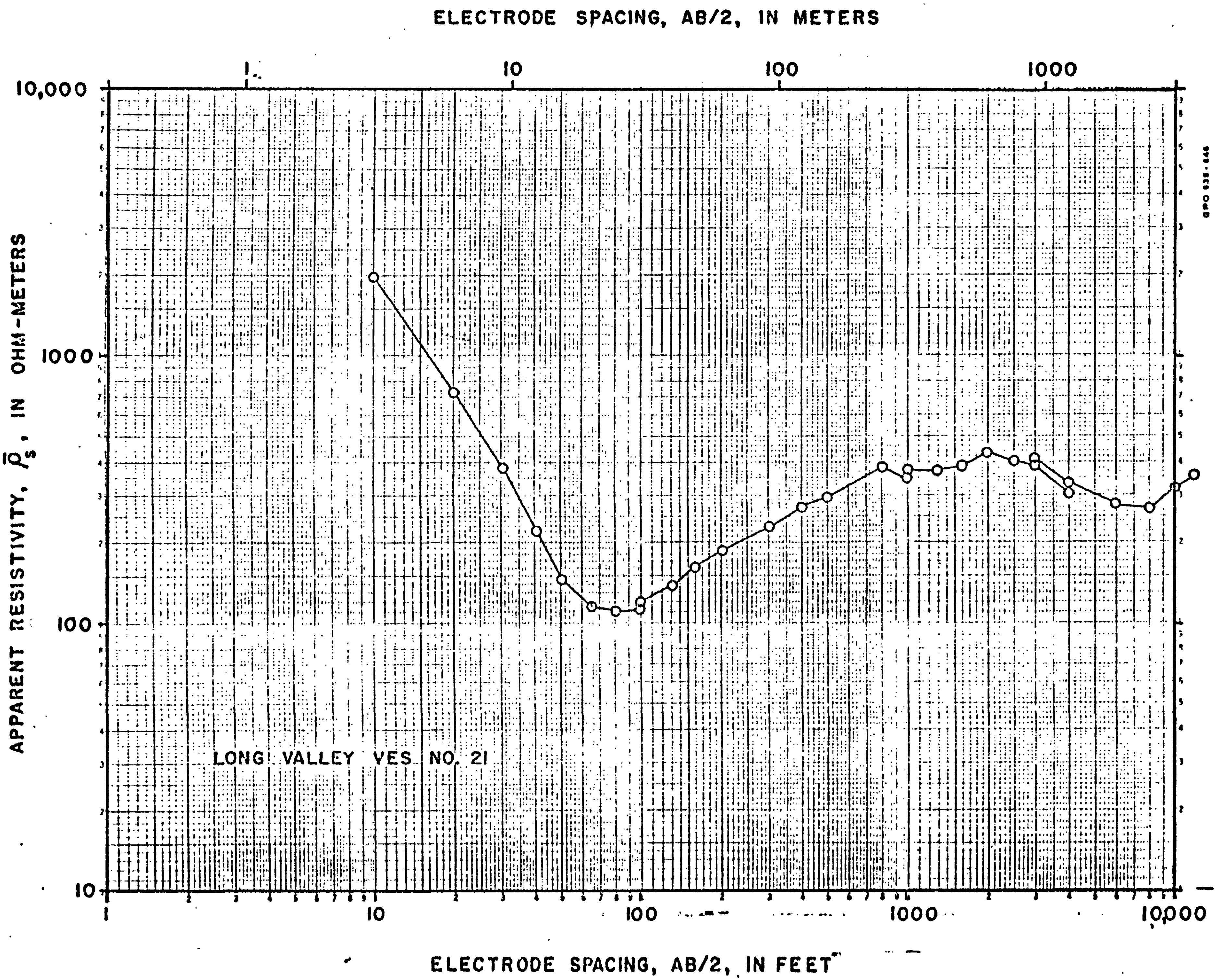

Figure 23.--Schlumberger sounding curve VES 21.

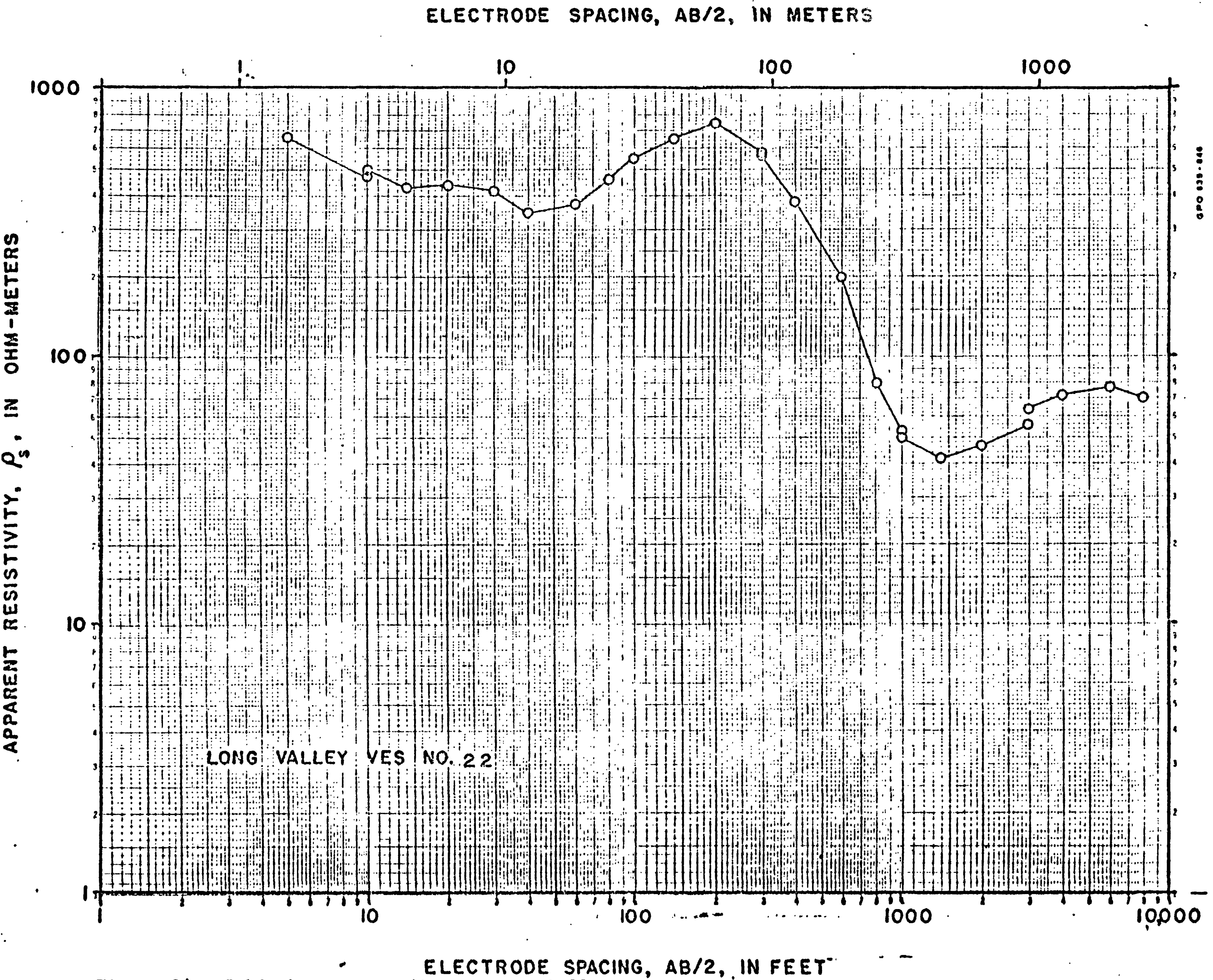

Figure 24.--Schlumberger sounding curve VES 22.

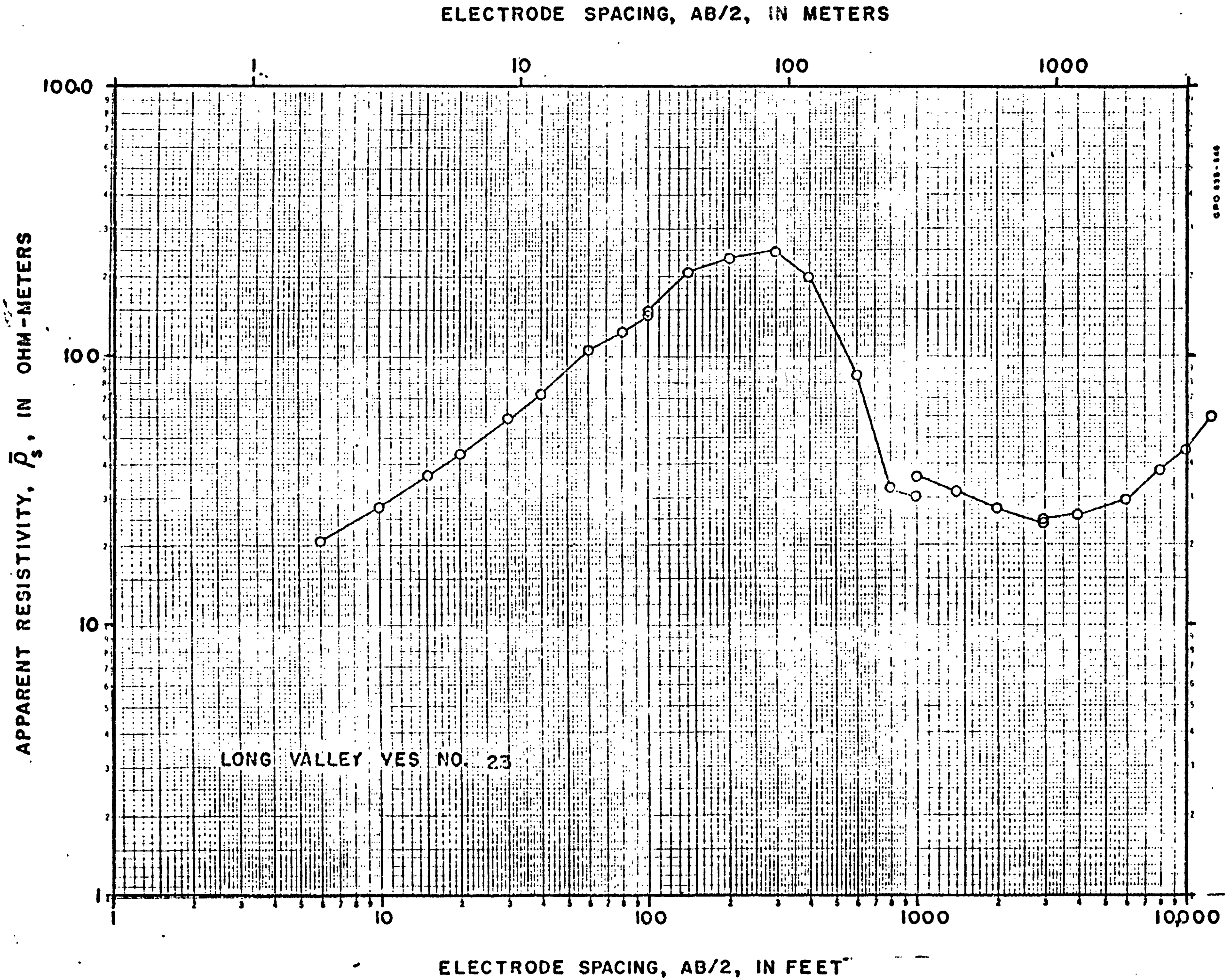

Figure 25.--Schlumberger sounding curve VES 23.

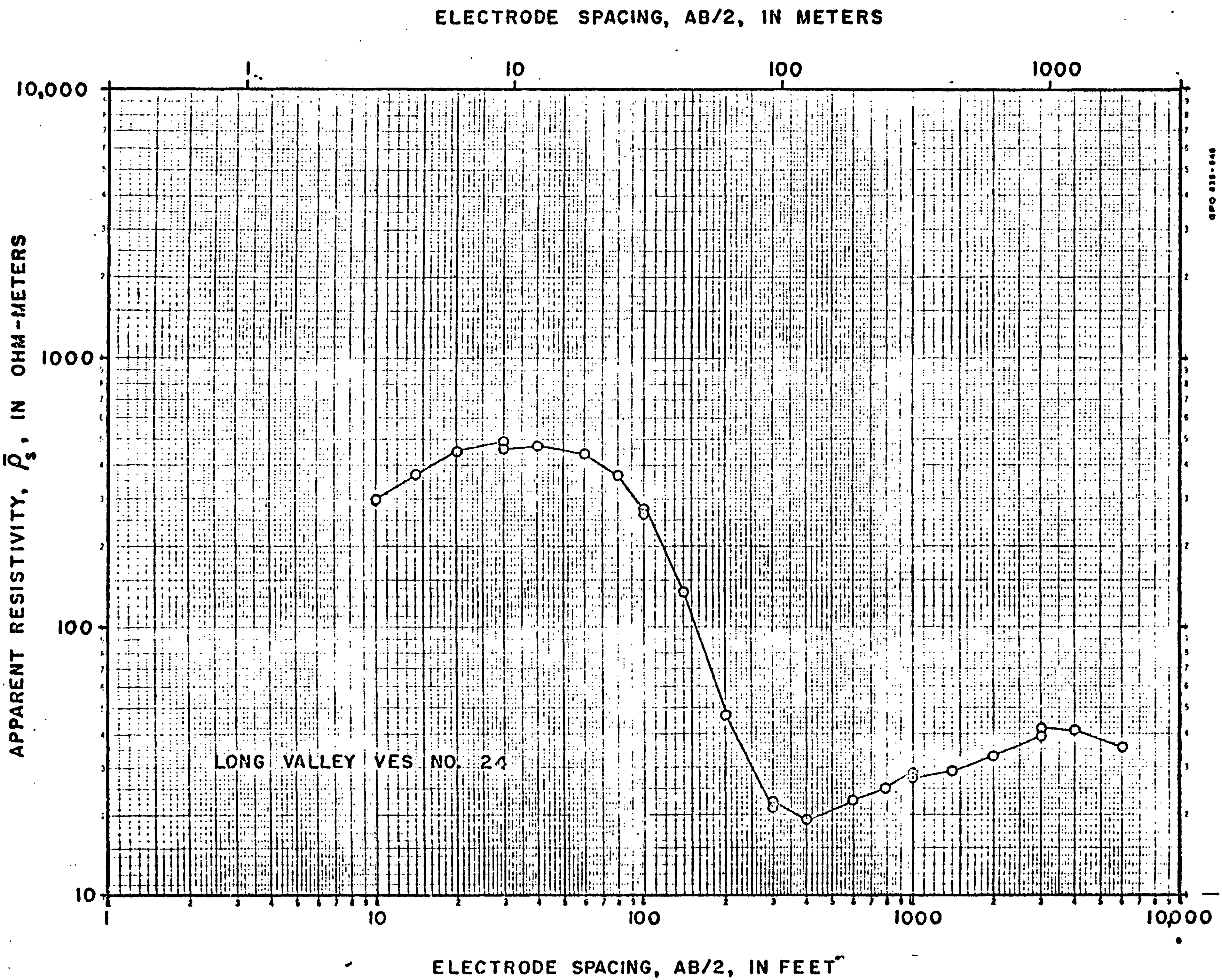

Figure 26.--Schlumberger sounding curve VES 24.

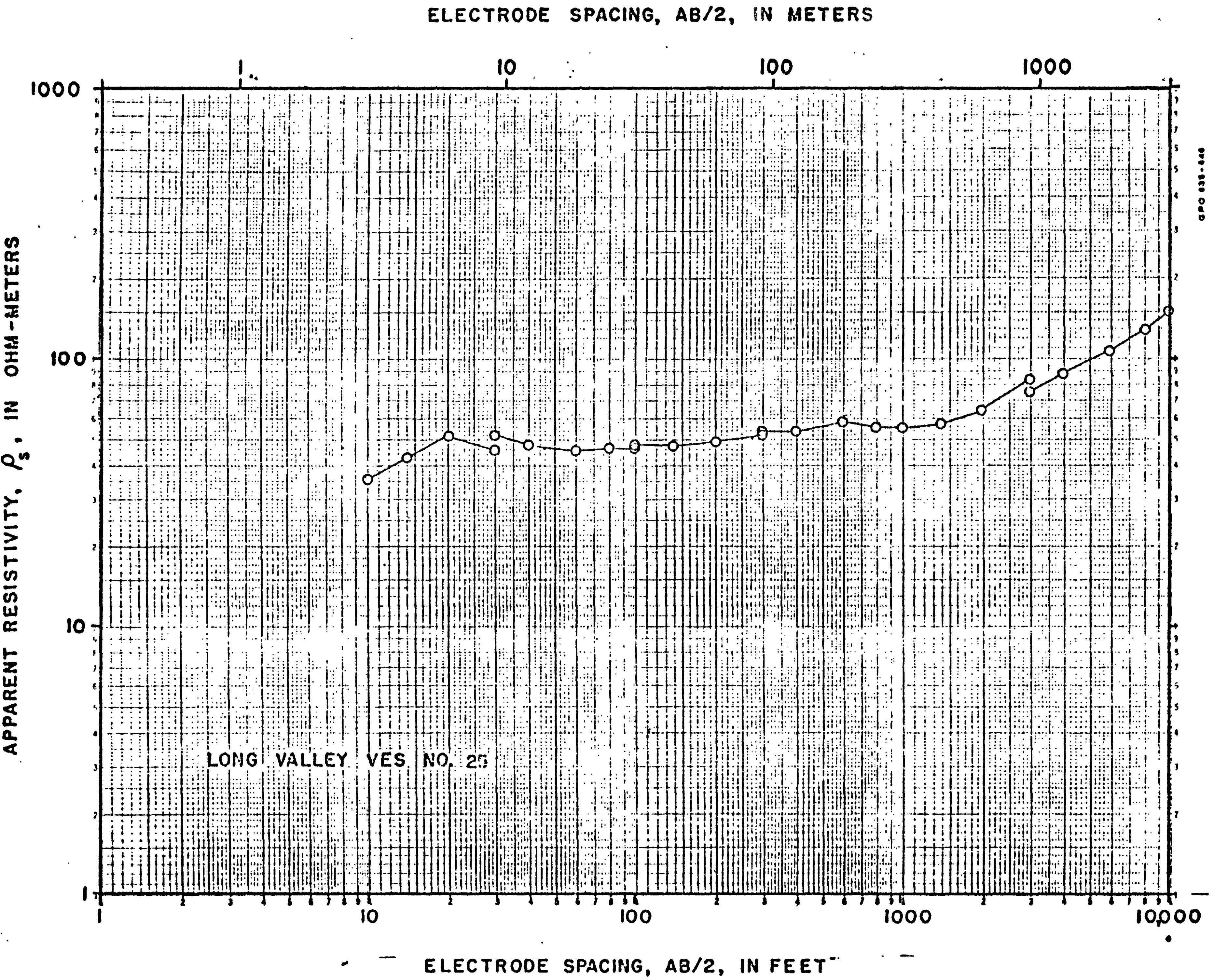

Figure 27.--Schlumberger sounding curve VES 25.

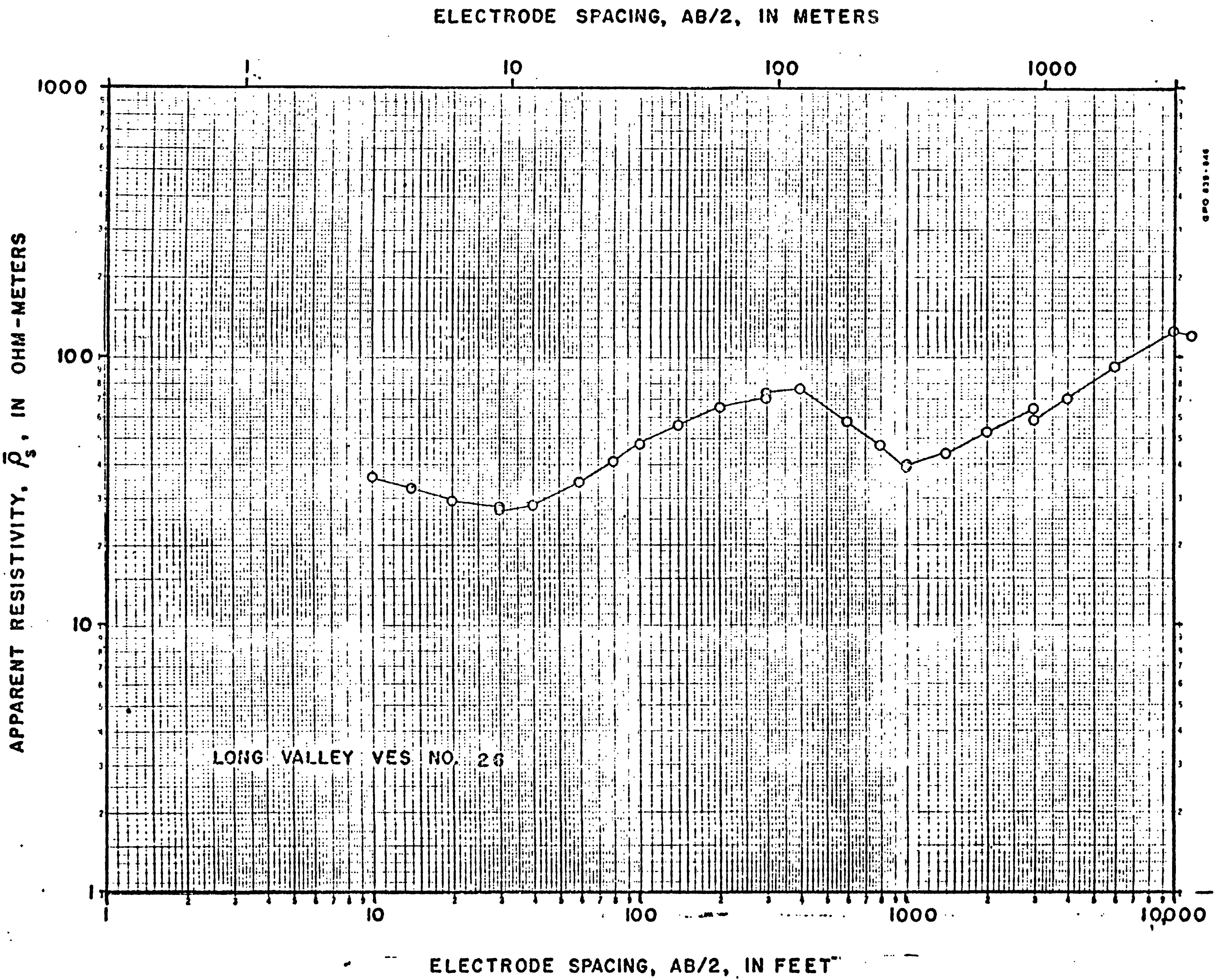

Figure 28.--Schlumberger sounding curve VES 26.

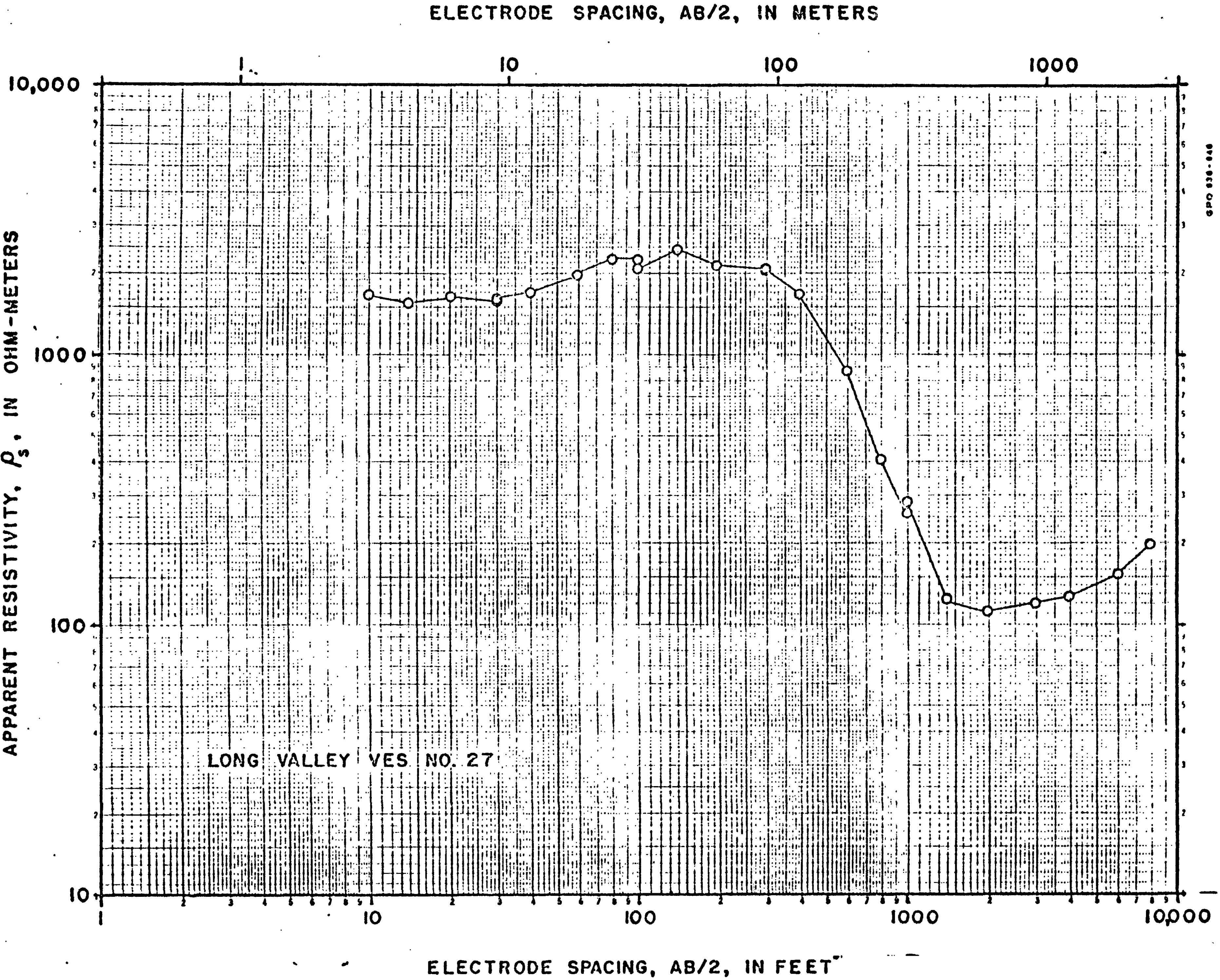

Figure 29.--Schlumberger sounding curve VES 27.

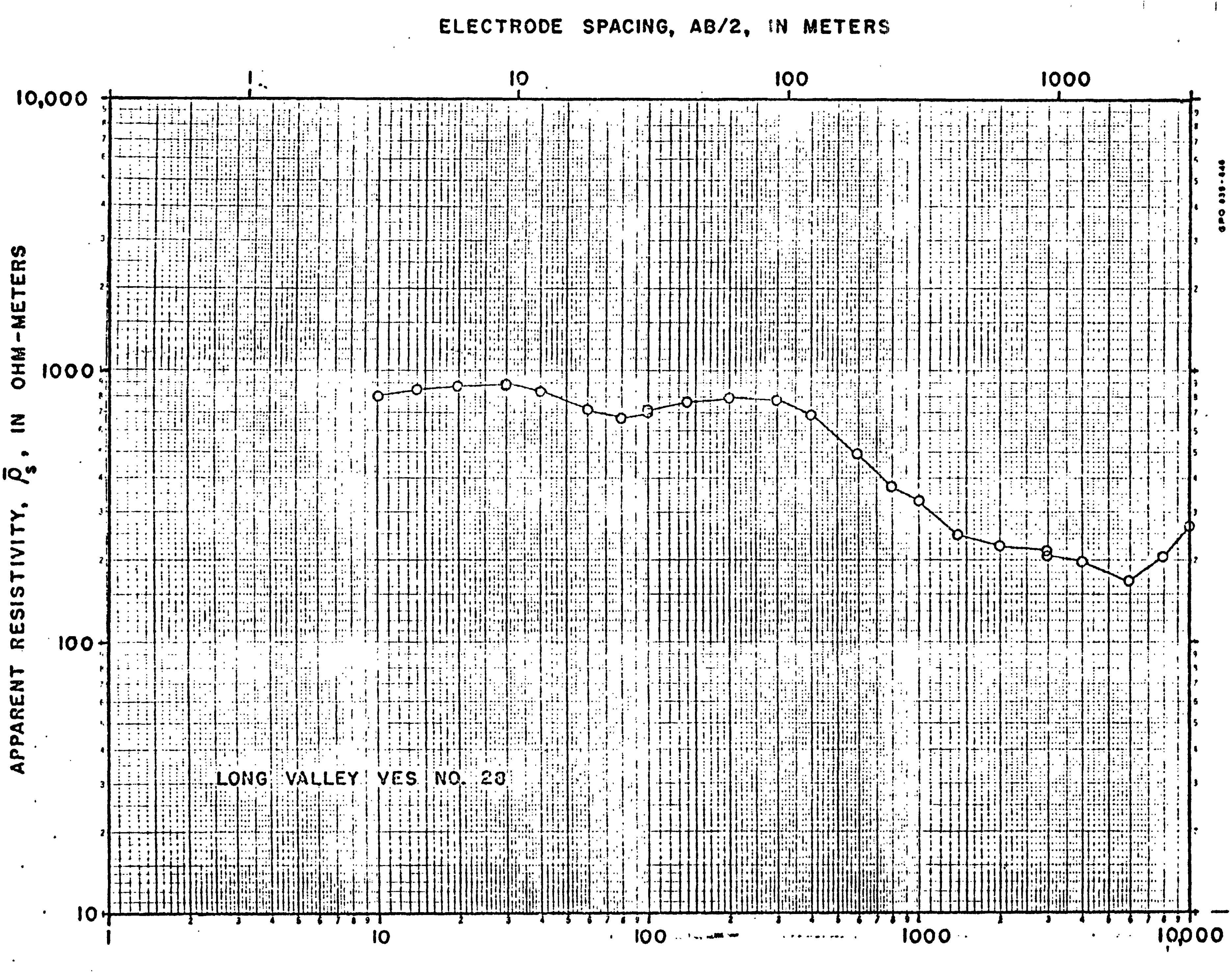

Figure 30.--Schlumberger sounding curve VES 28.

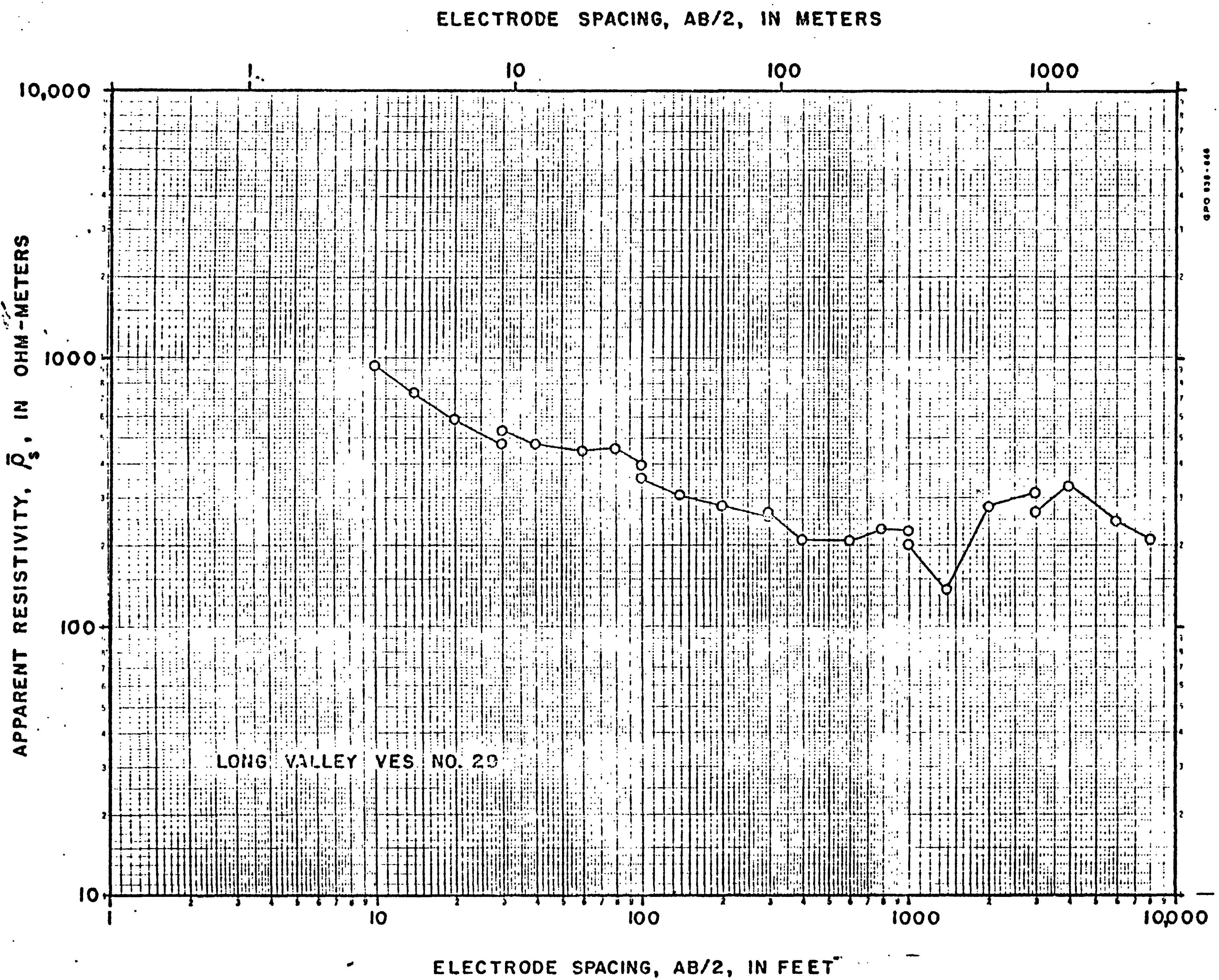

Figure 31.--Schlumberger sounding curve VES 29.

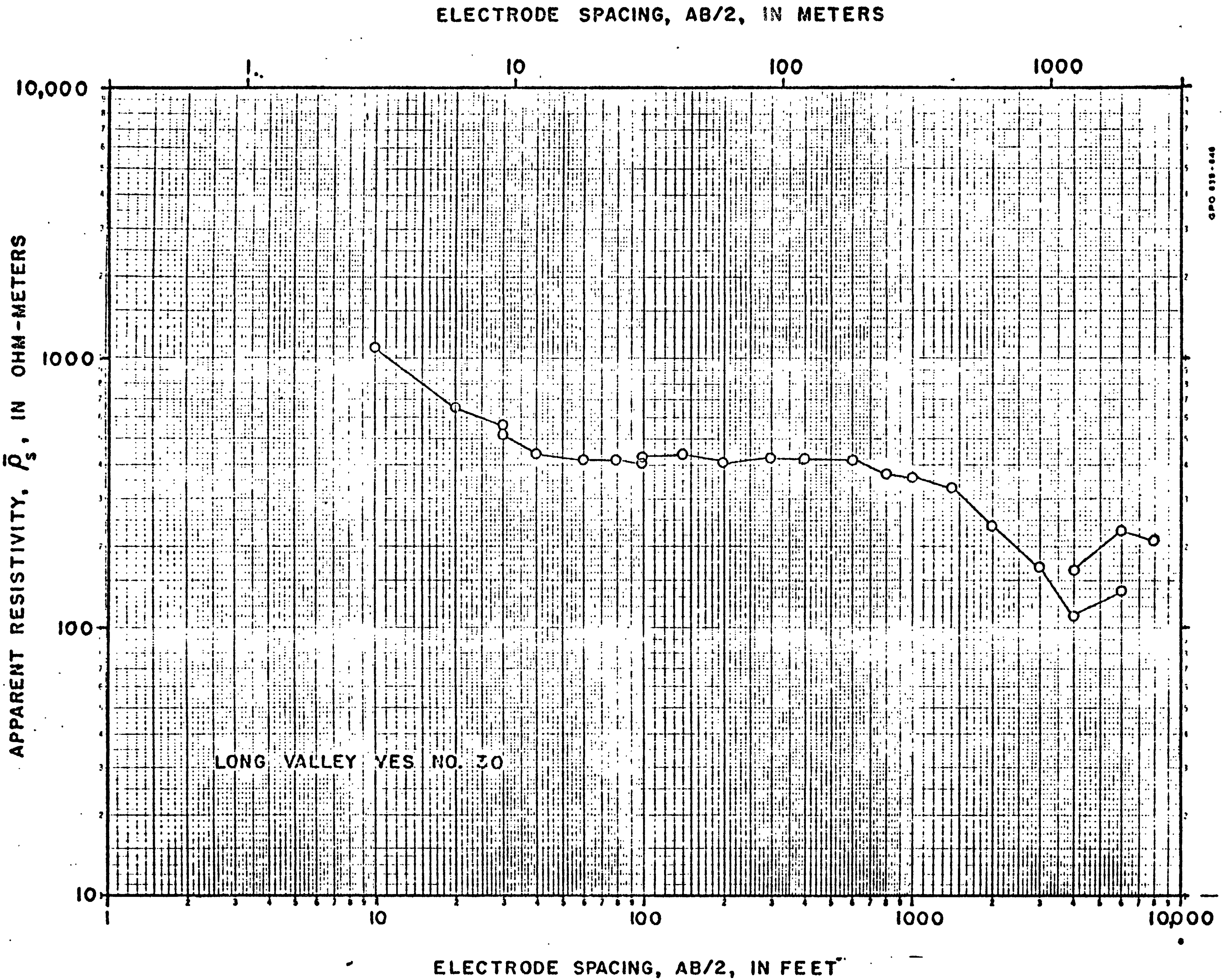

Figure 32.--Schlumberger sounding curve VES 30.

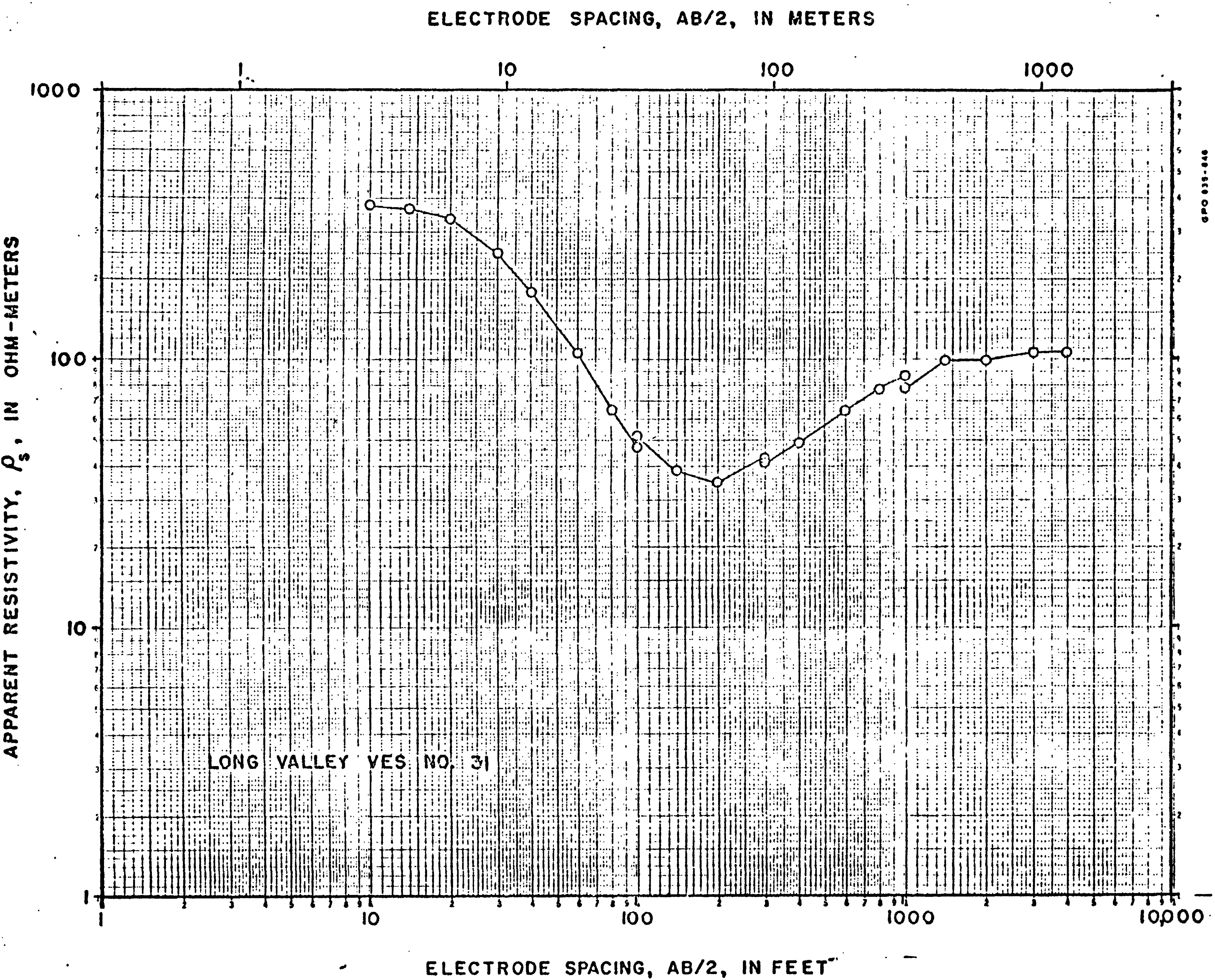

Figure 33.--Schlumberger sounding curve VES 31.

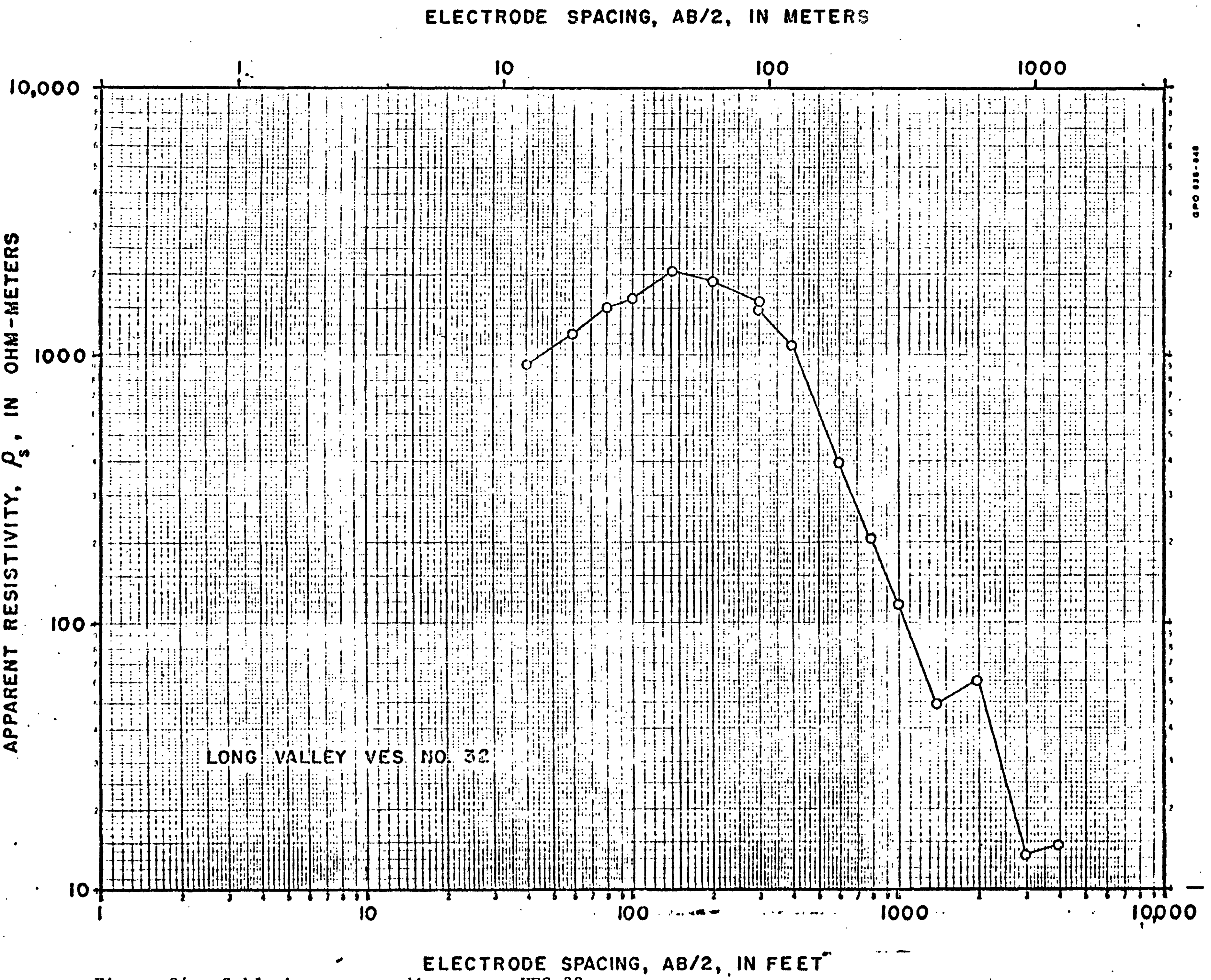

Figure 34.--Schlumberger sounding curve VES 32.

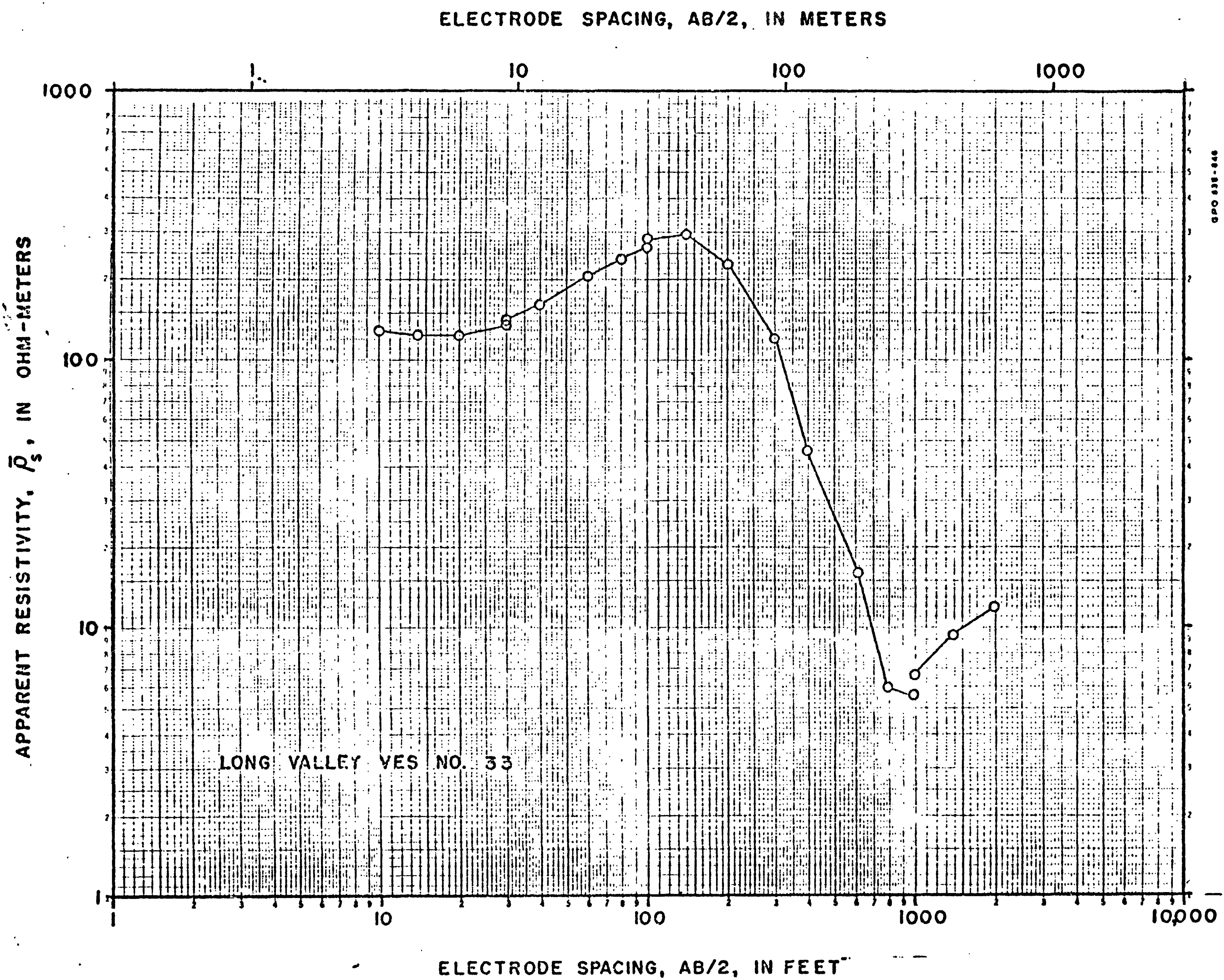

Figure 35.--Schlumberger sounding curve VES 33.

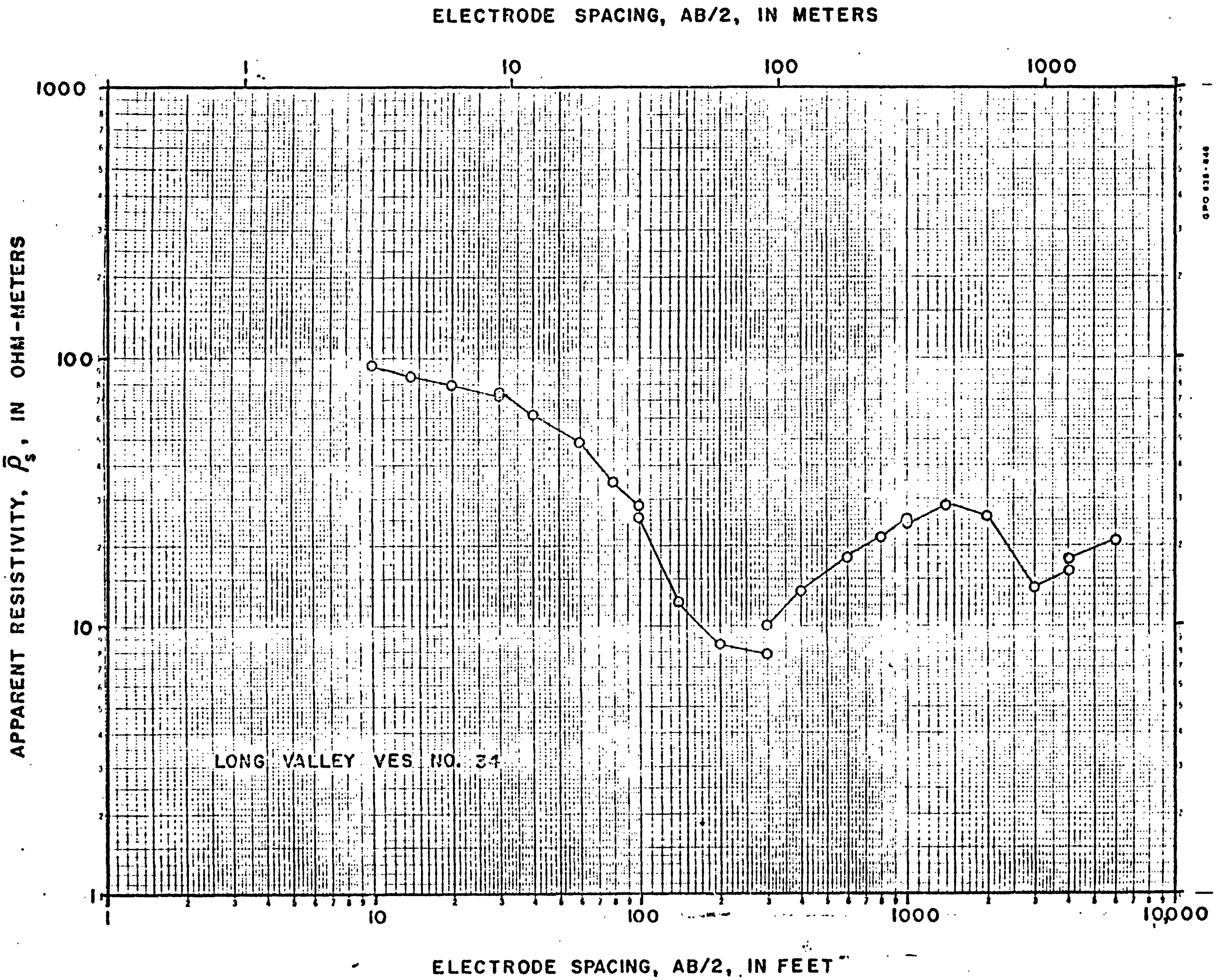

Figure 36.--Schlumberger sounding curve VES 34.

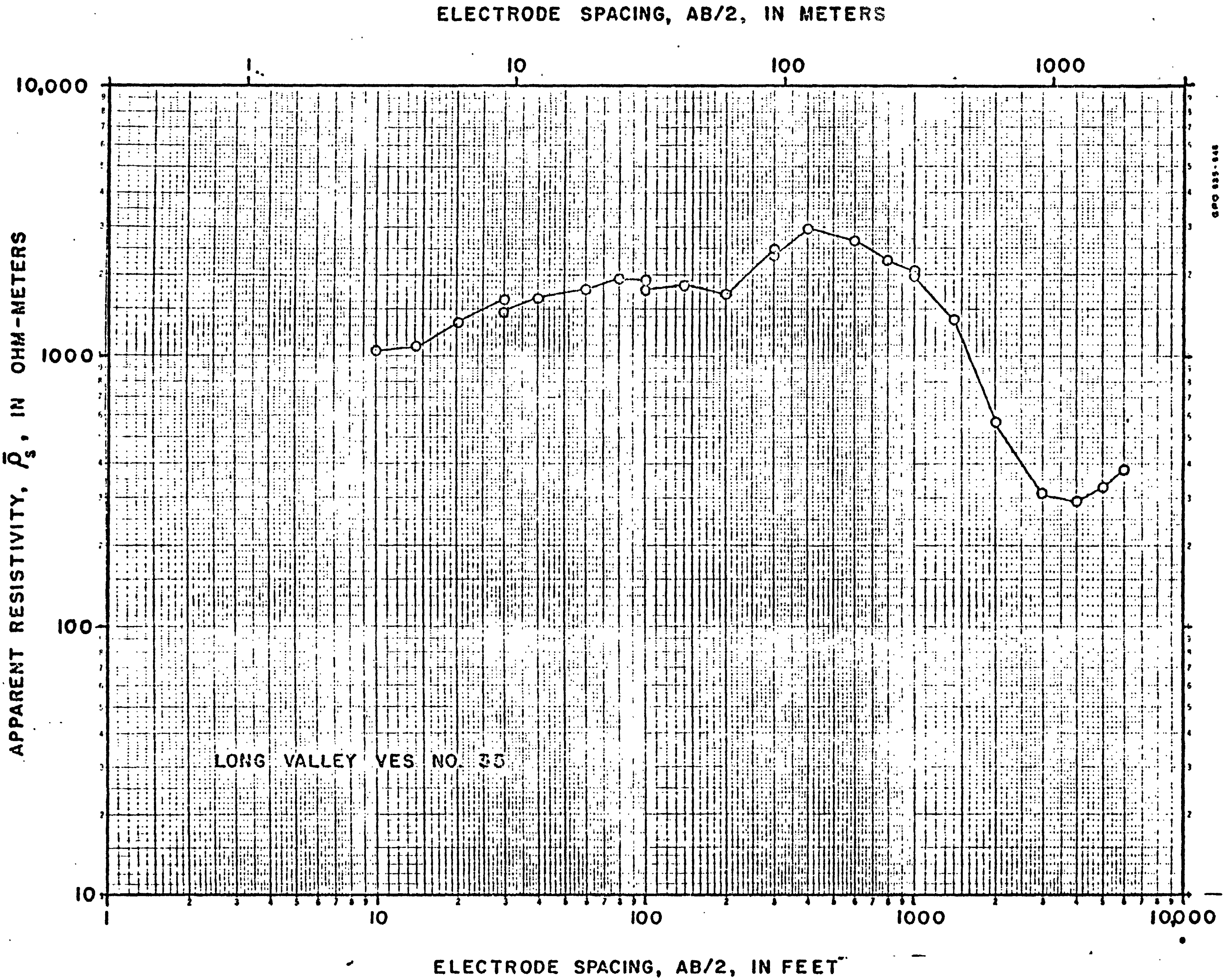

Figure 37.--Schlumberger sounding curve VES 35.

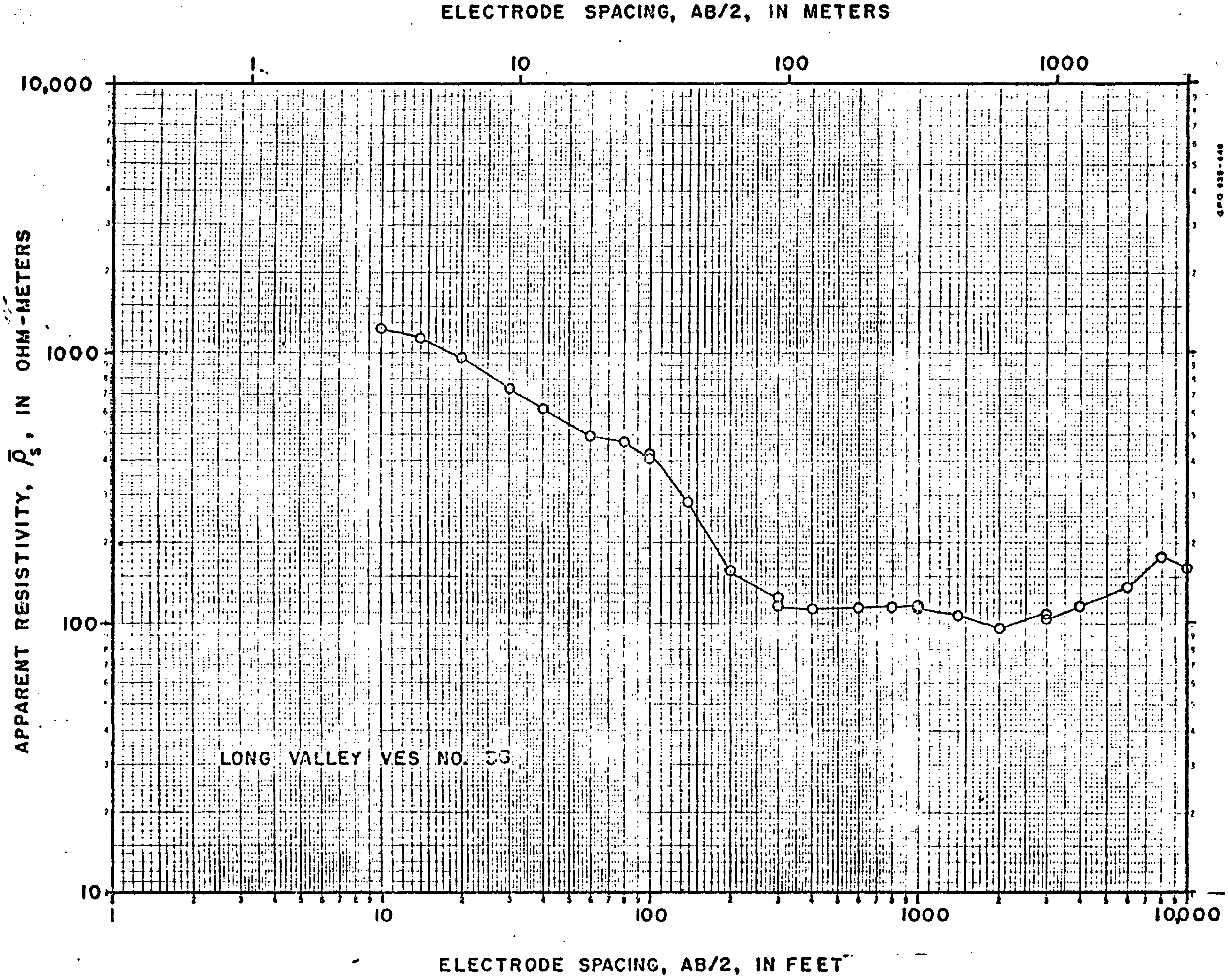

Figure 38.--Schlumberger sounding curve VES 36.

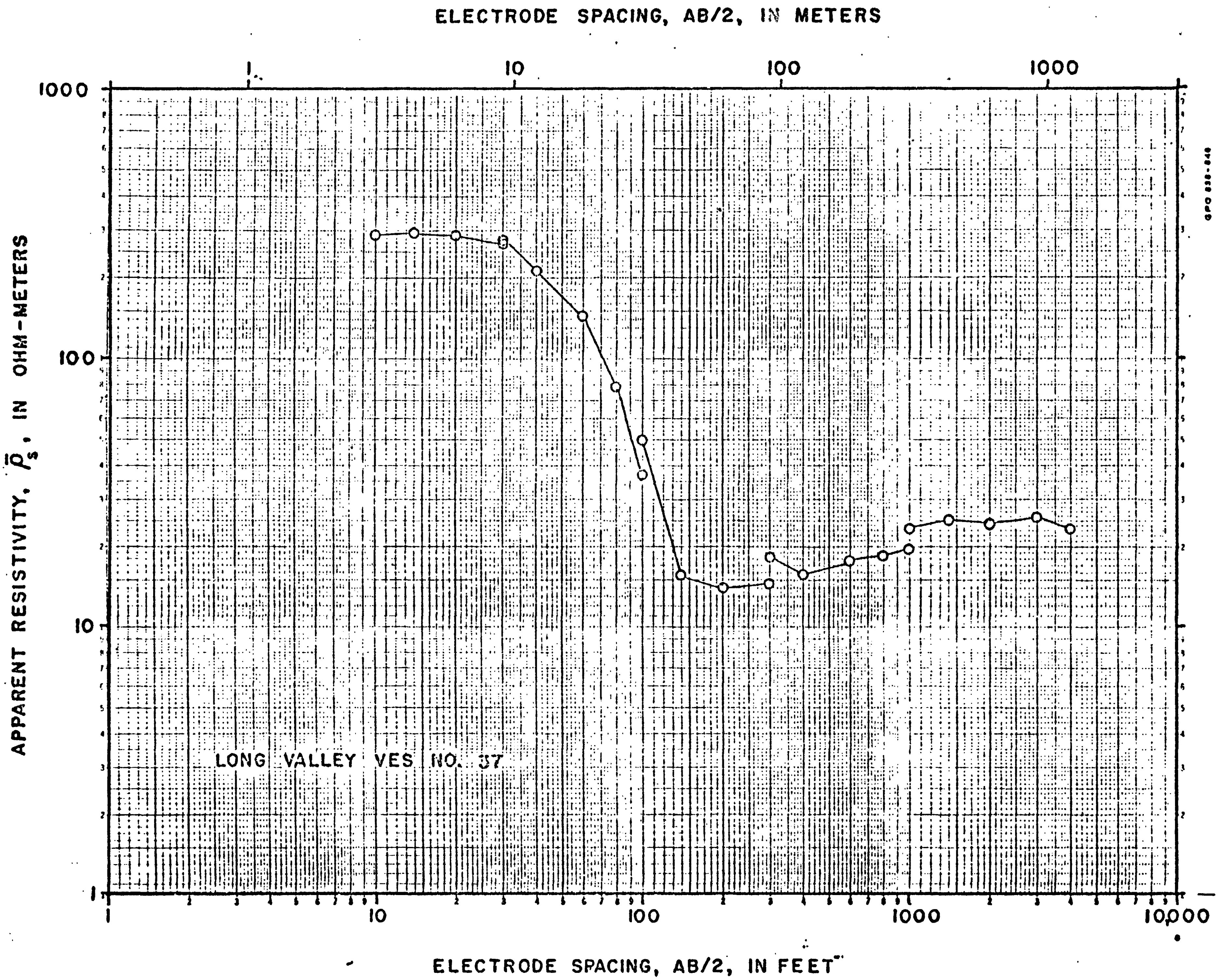

Figure 39.--Schlumberger sounding curve VES 37.

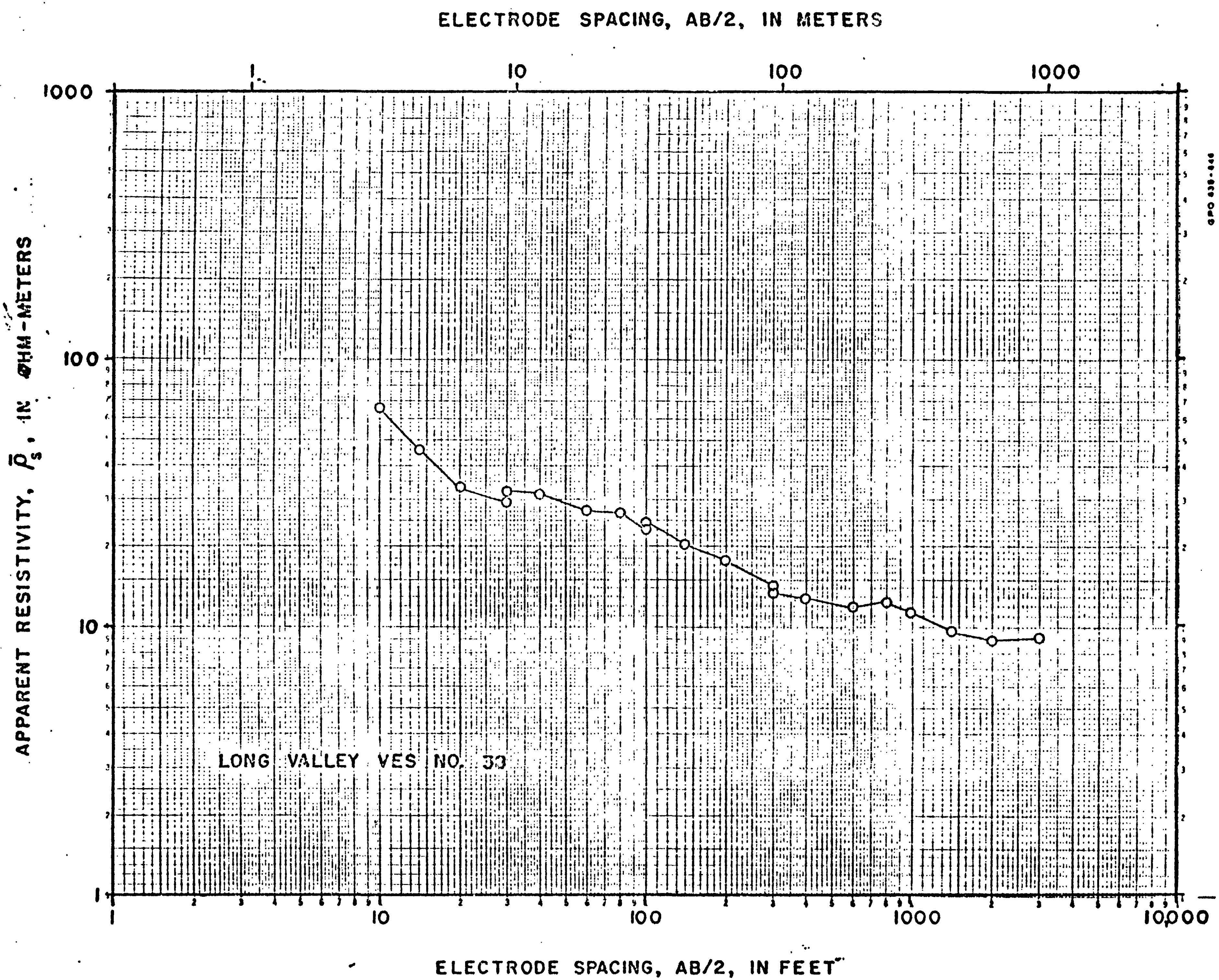

Figure 40.--Schlumberger sounding curve VES 38.

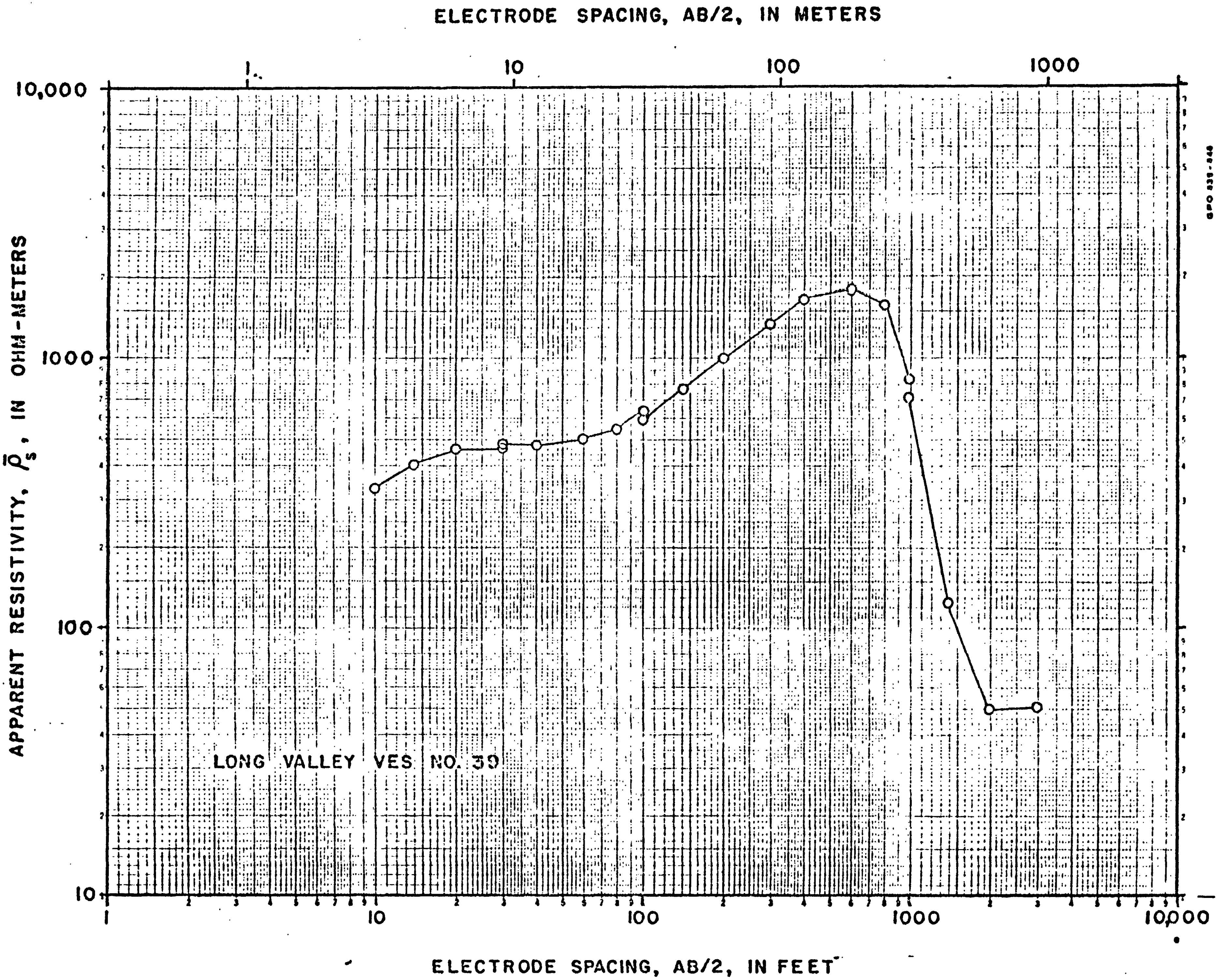

Figure 41.--Schlumberger sounding curve VES 39.

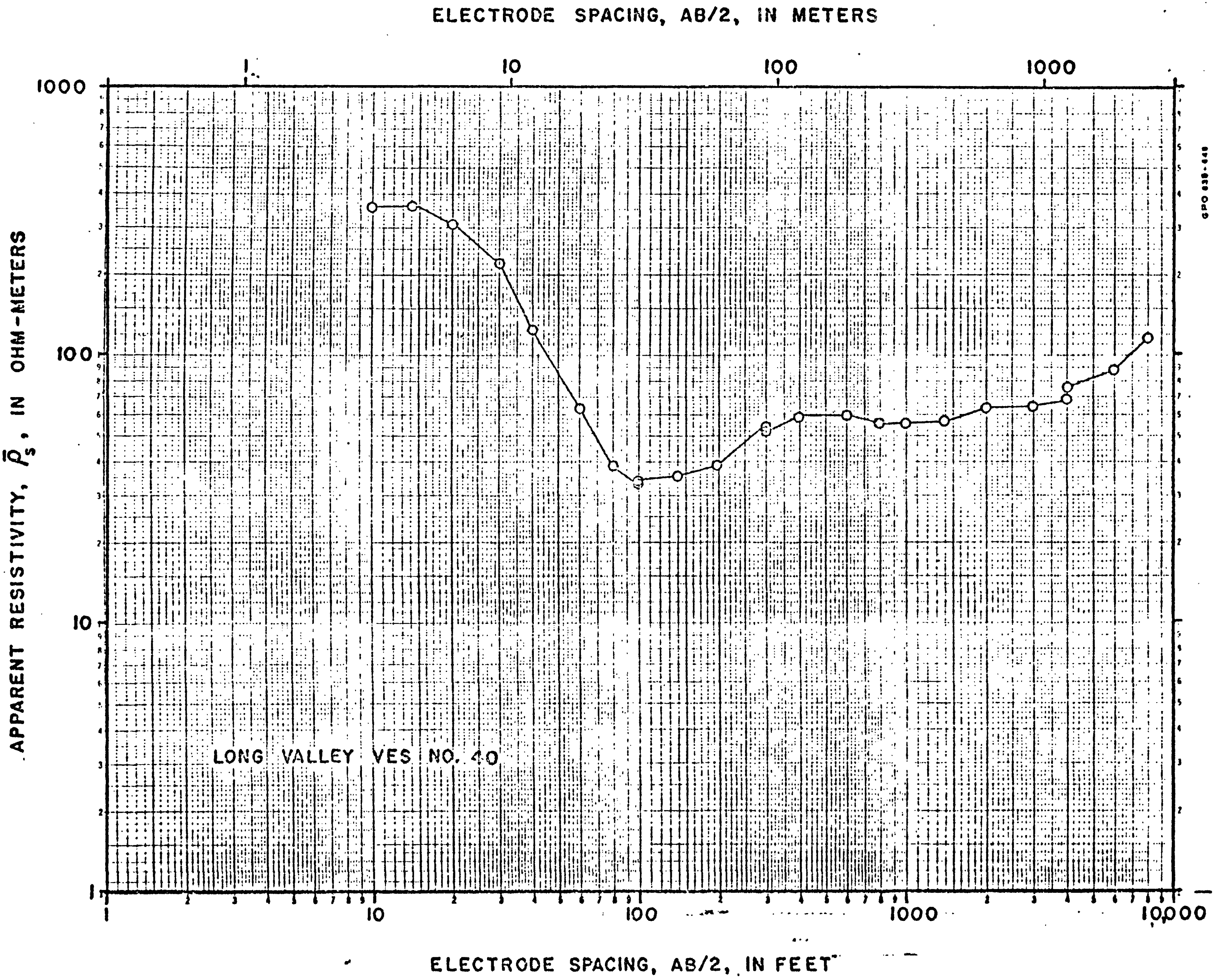

Figure 42.--Schlumberger sounding curve VES 40.

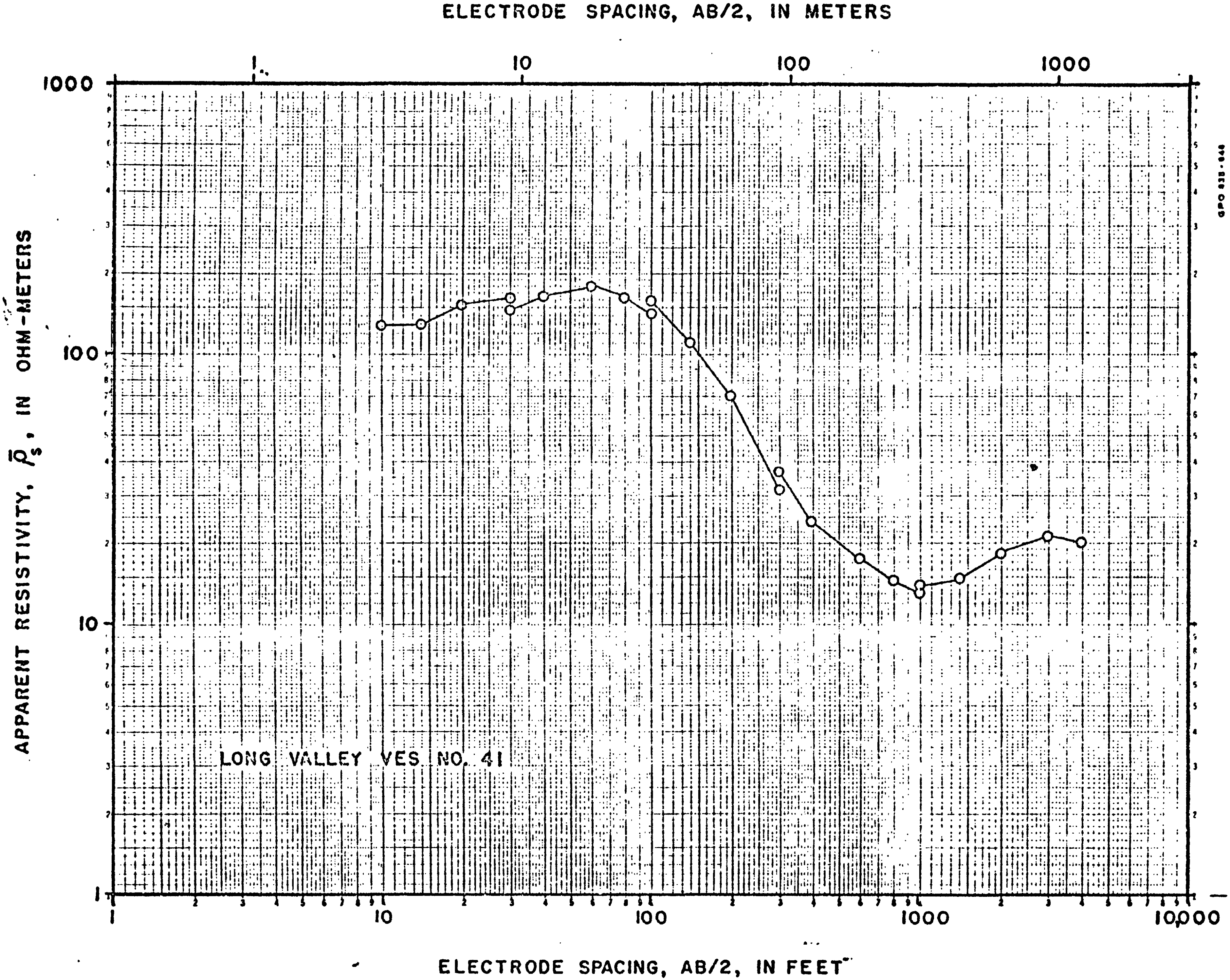

Figure 43.--Schlumberger sounding curve VES 41.

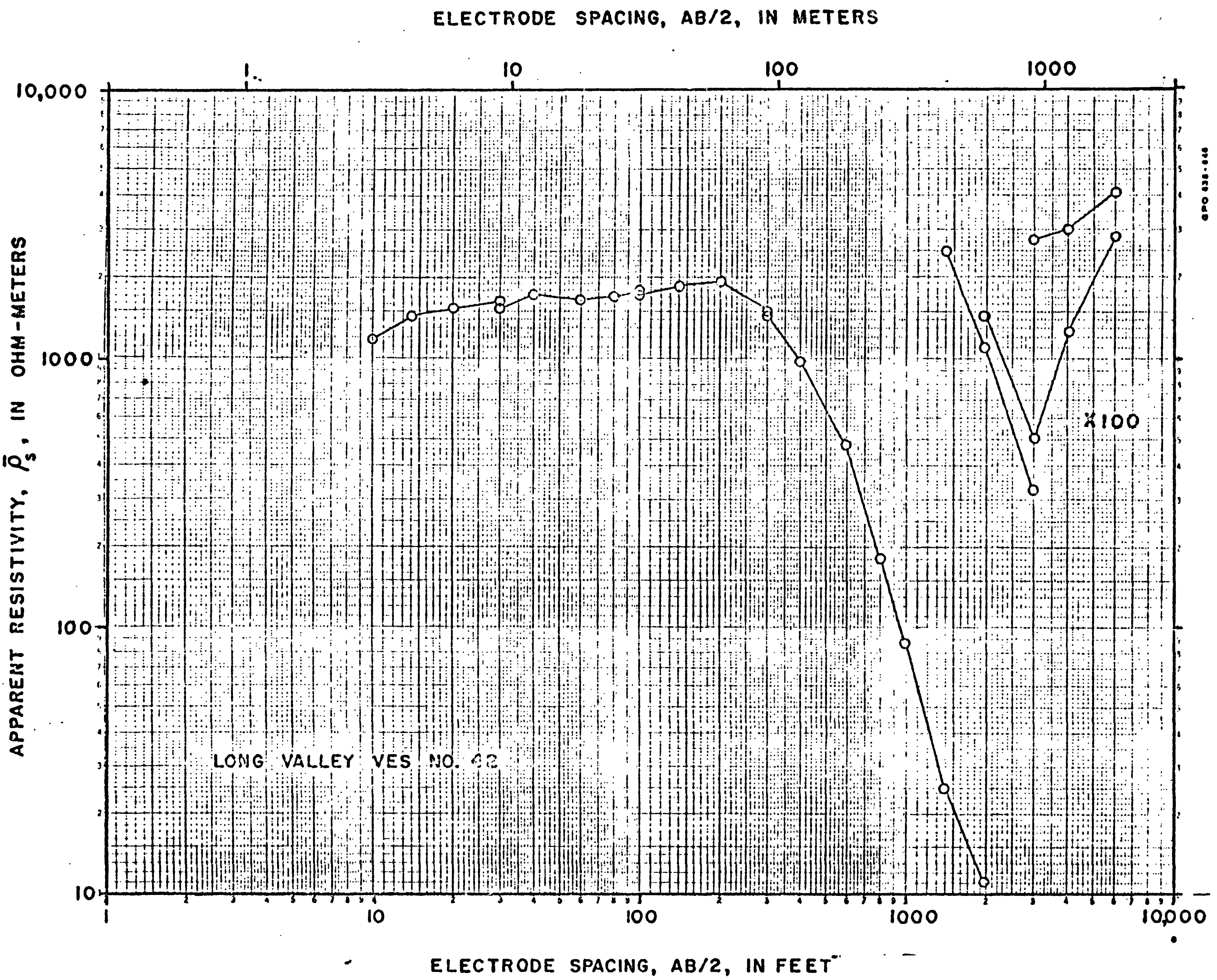

Figure 44.--Schlumberger sounding curve VES 42.

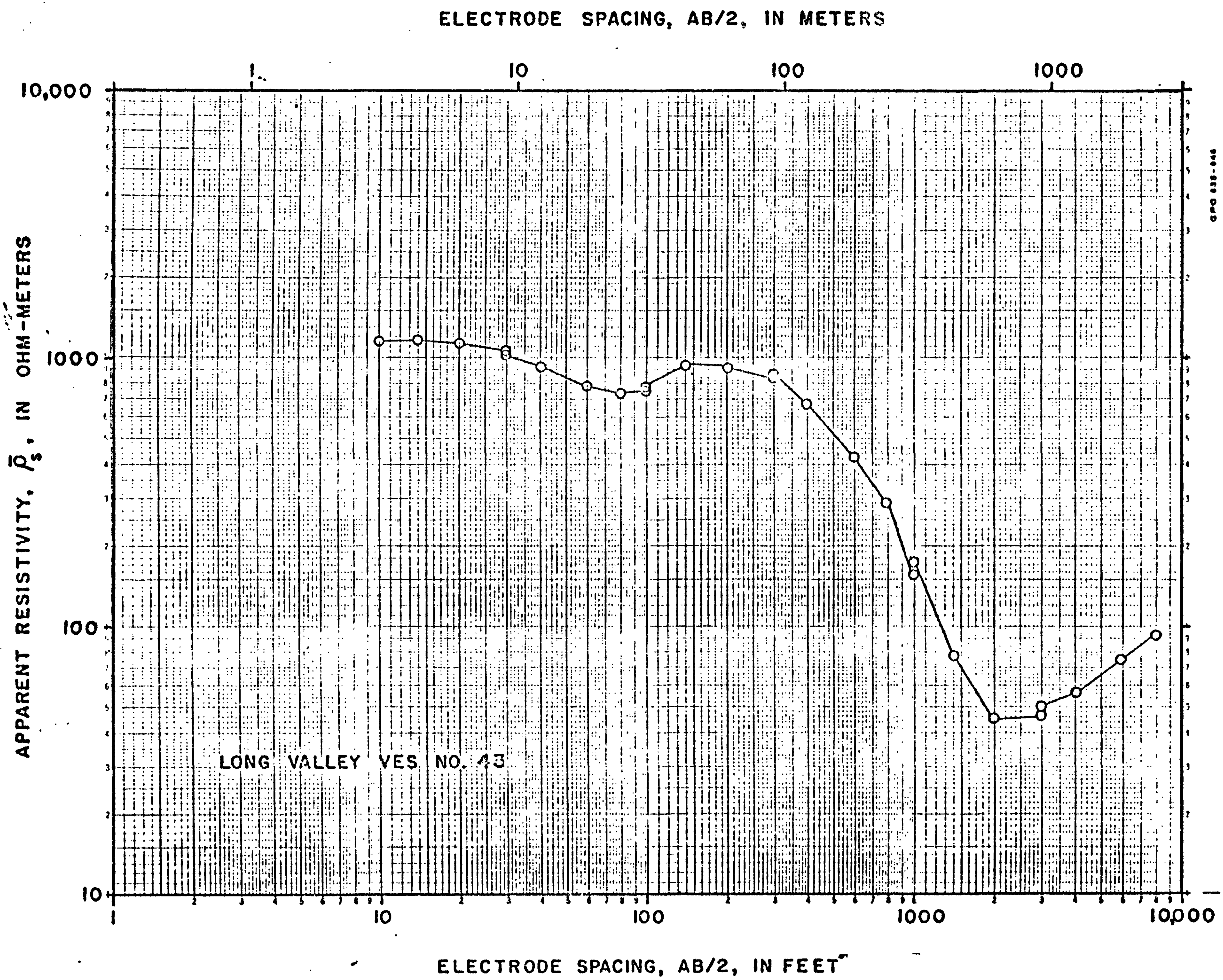

Figure 45.--Schlumberger sounding curve VES 43.

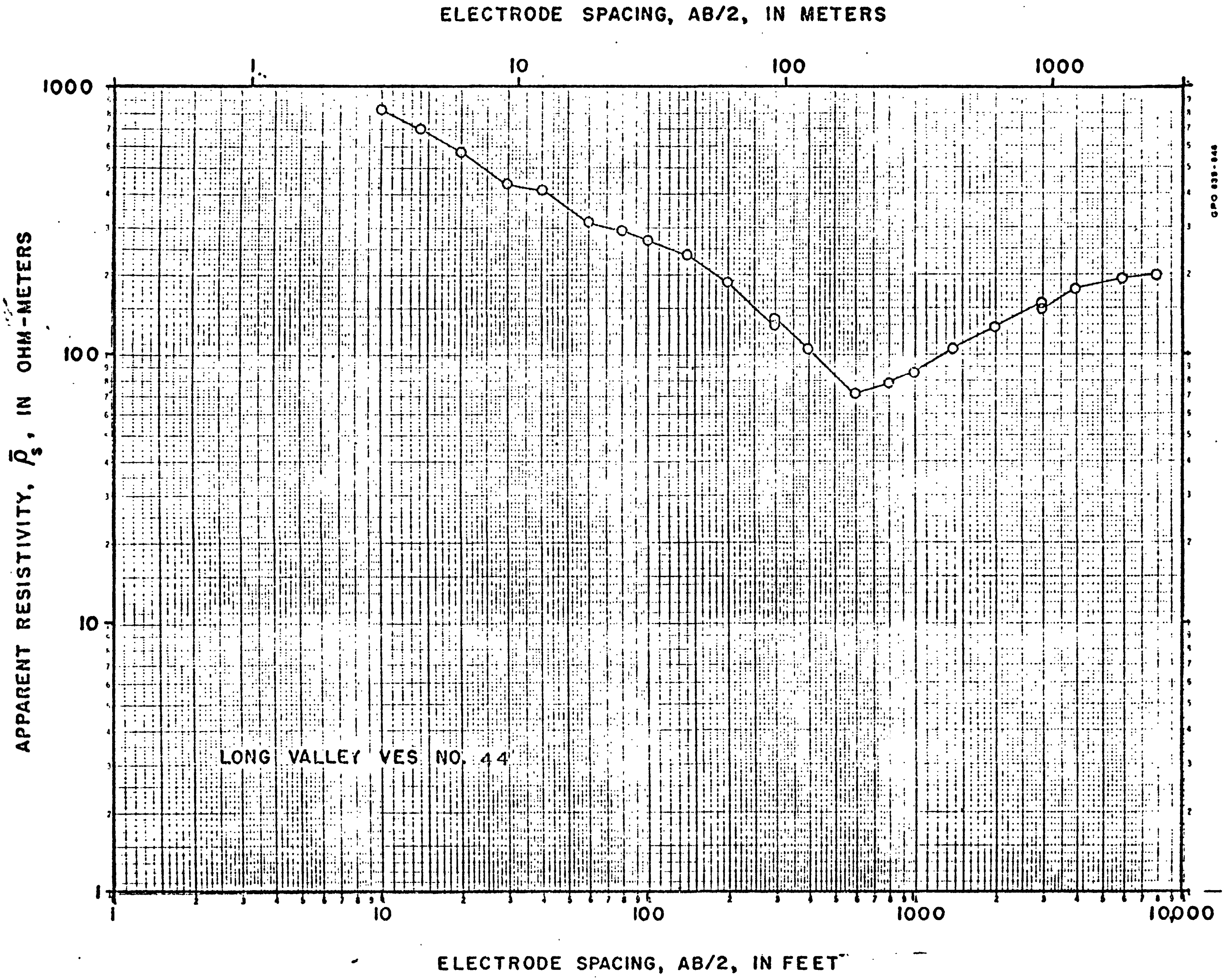

Figure 46.--Schlumberger sounding curve VES 44.

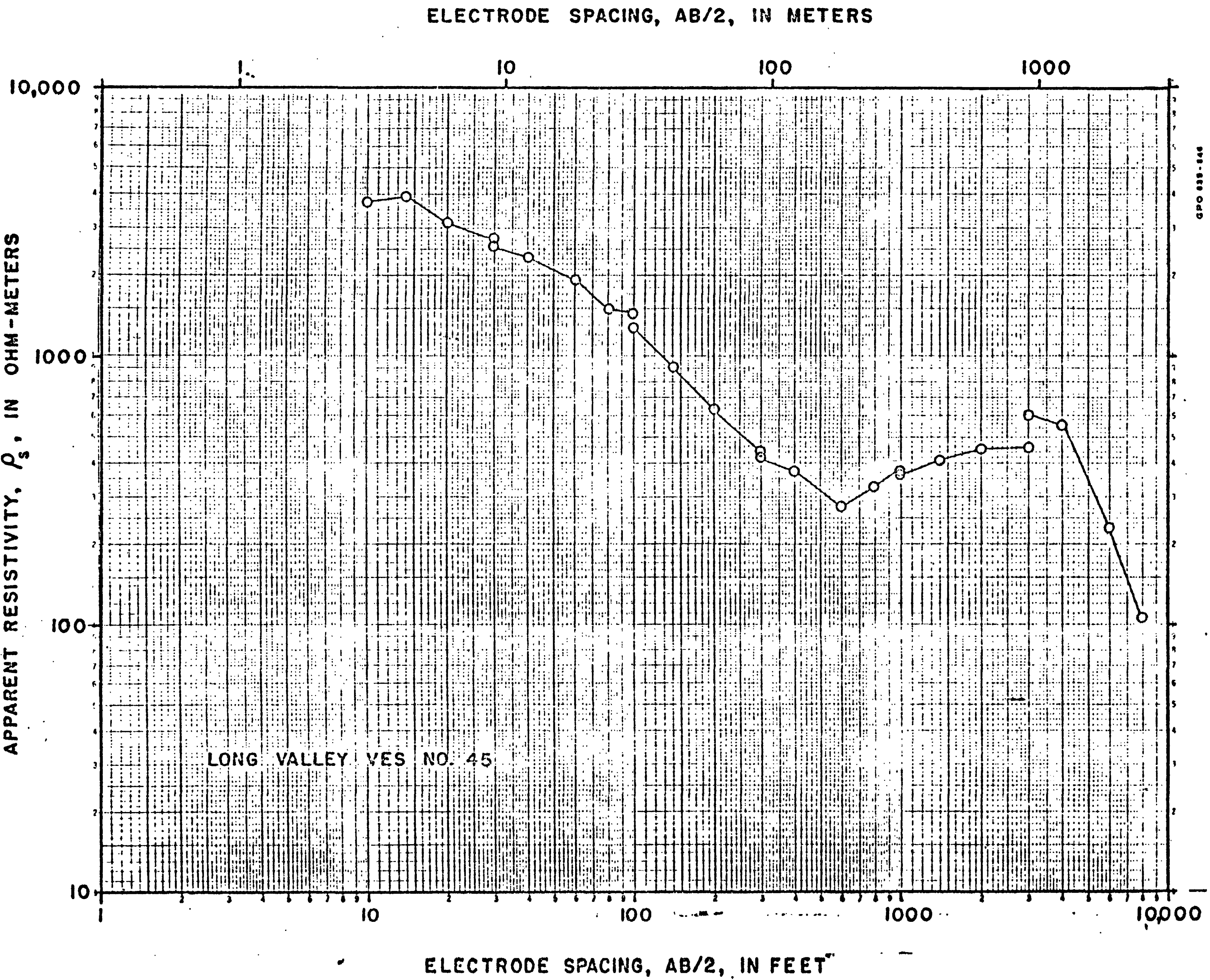

Figure 47.--Schlumberger sounding curve VES 45.

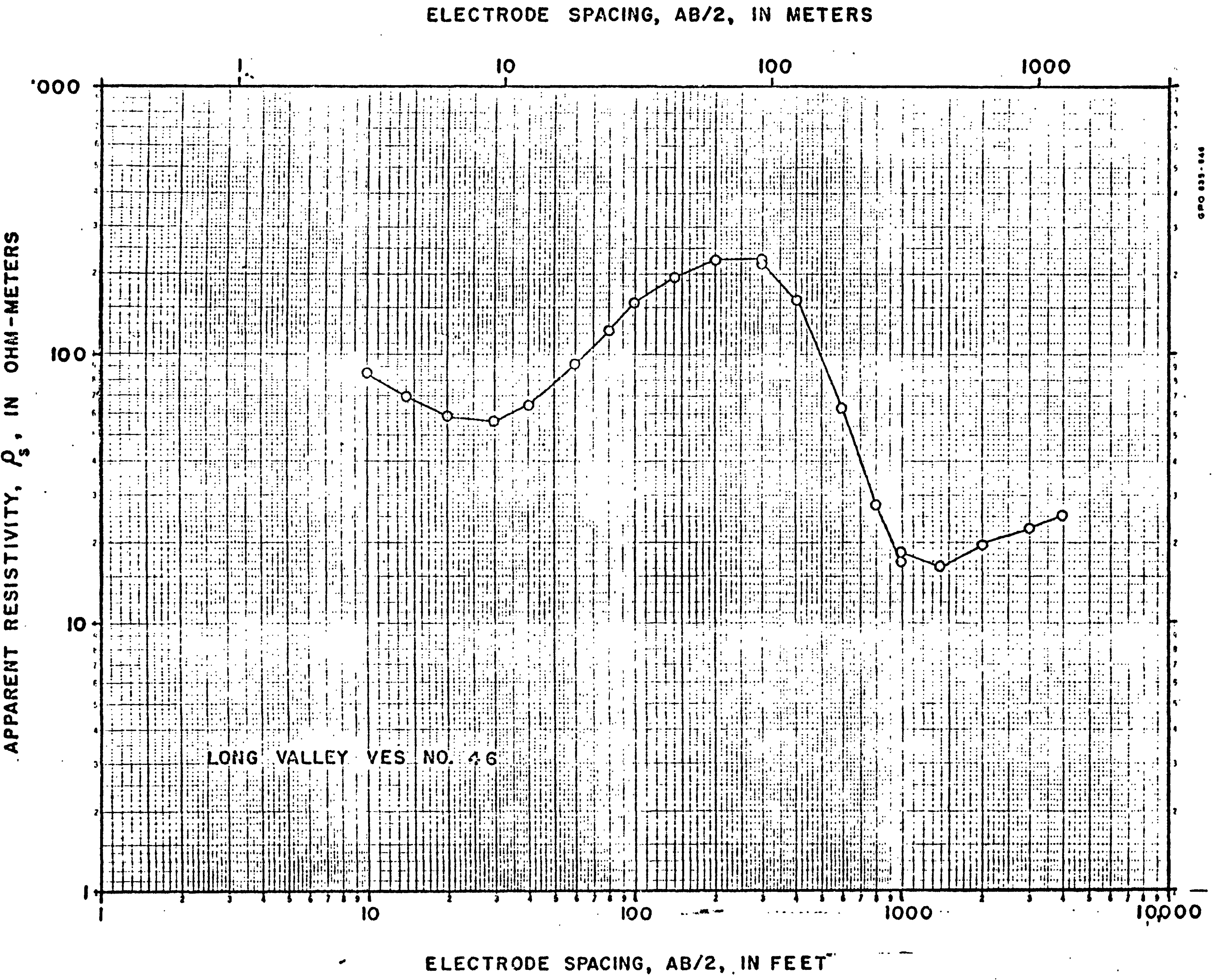

Figure 48.--Schlumberger sounding curve VES 46.

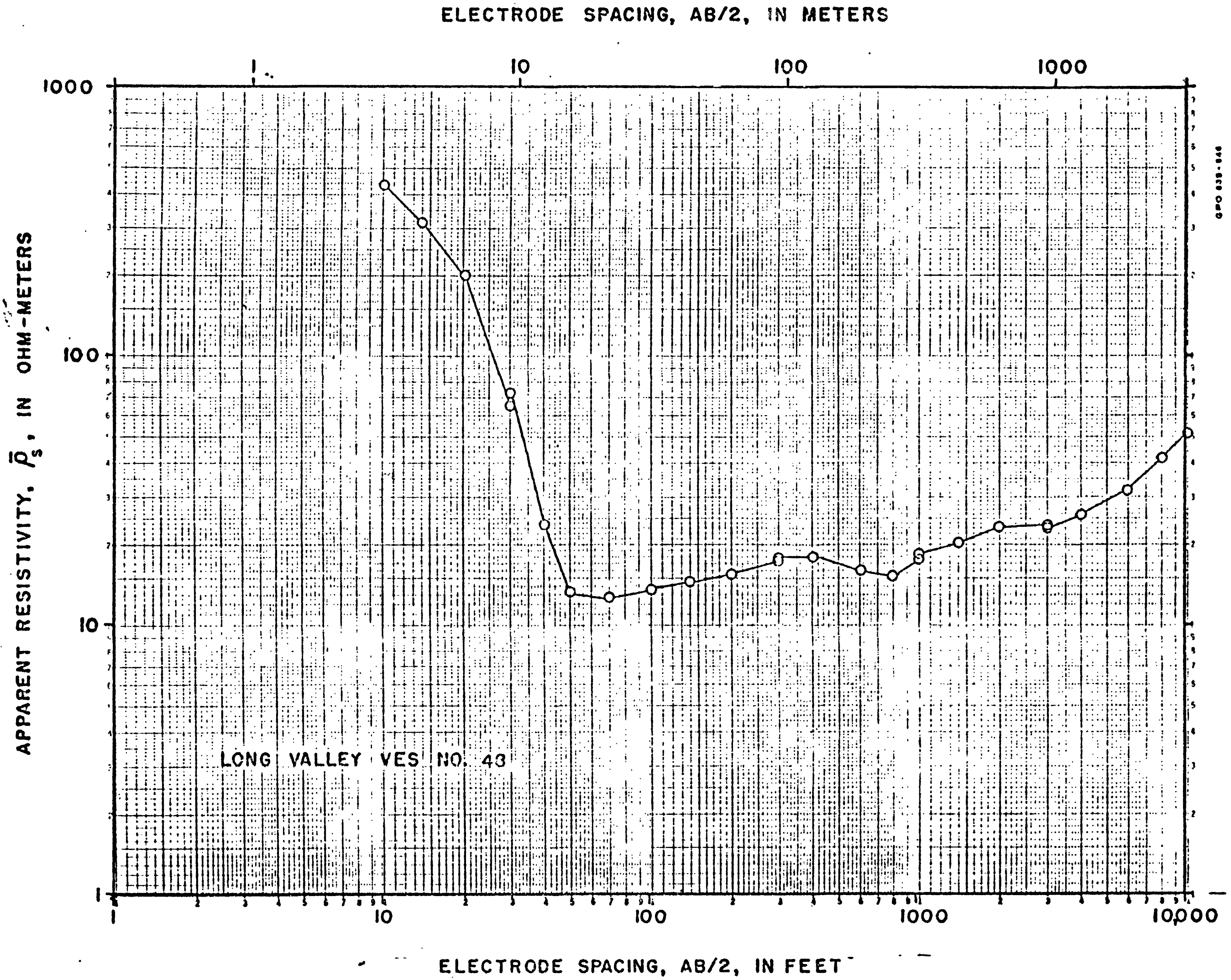

Figure 49.--Schlumberger sounding curve VES 48.

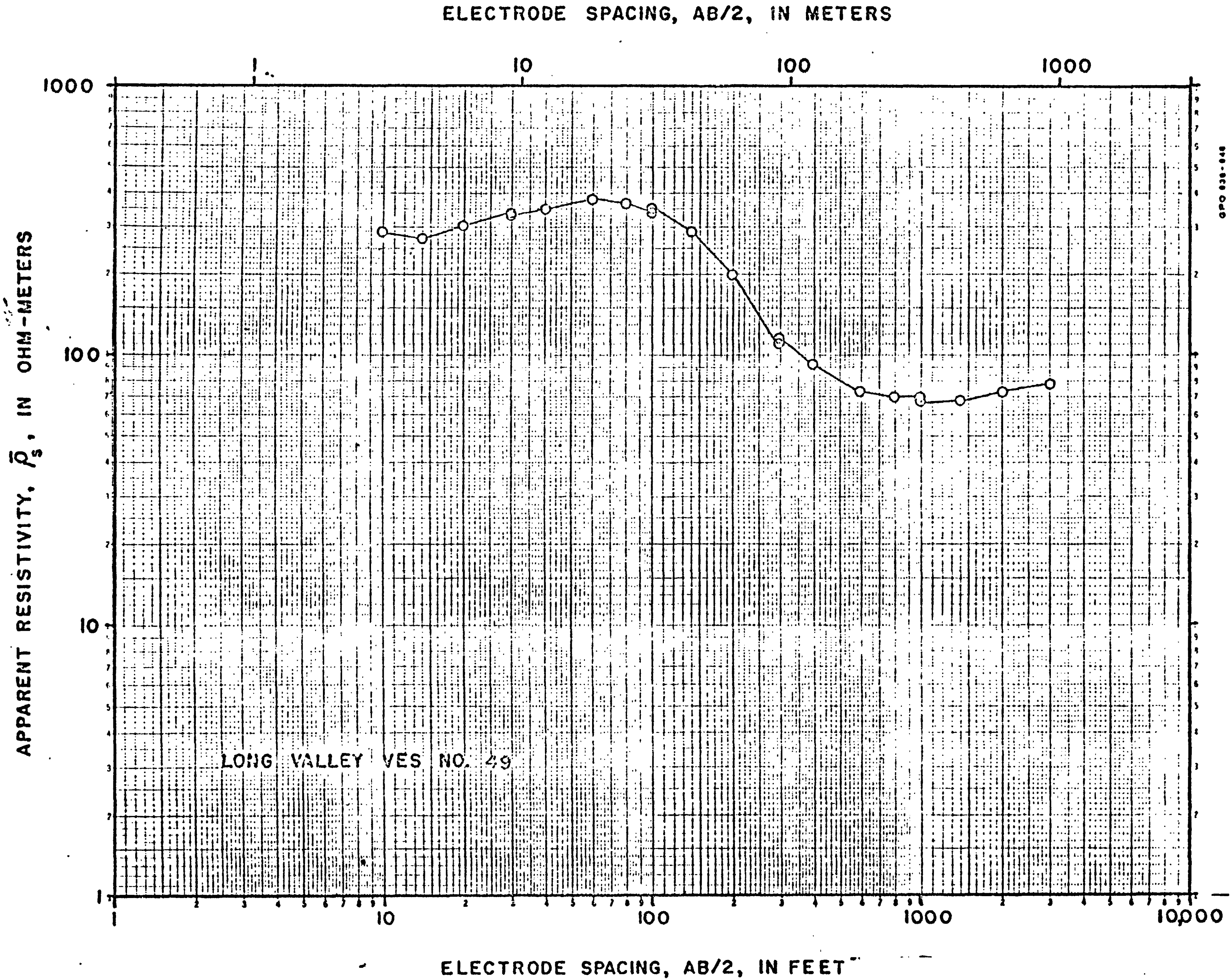

Figure 50.--Schlumberger sounding curve VES 49.

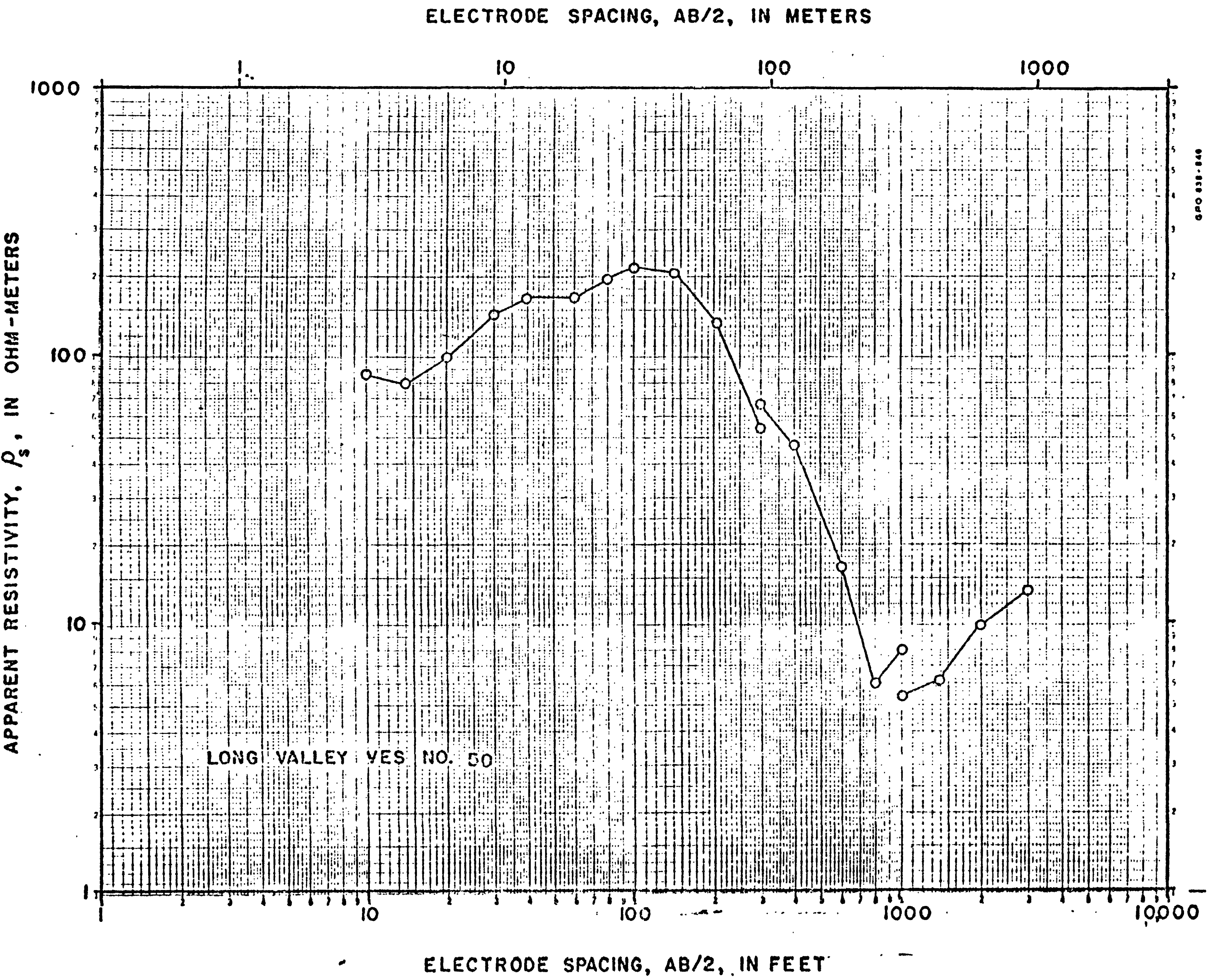

Figure 51.--Schlumberger sounding curve VES 50.

1973). Plate 10 shows pseudo-electric logs from VES 7 and VES 8 and an induction and temperature log from test hole LV1. On plate 9, the 45-100 ohm-meter material beneath, and east of, the tuff is probably post-caldera rhyolite or possibly intra-caldera flow units and may include the Bishop Tuff, which has an interpreted resistivity of 85 ohm-meters at a location outside the caldera (fig. 52). The lowermost resistive layer detected on VES 26 and VES 28 may be either downfaulted Glass Mountain rhyolitic volcanics or other pre-caldera rocks, although gravity data (Pakiser and others, 1964) and seismic refraction data (D. G. Hill, oral commun., 1973) indicate that the floor of the caldera is much deeper than 1.5 km as shown at VES 28. The near-surface units of 10-45 ohm-meter resistivity probably represent Pleistocene lake sediments. The indicated structural activity beneath VES 9 may represent the major source of thermal waters which invaded and altered the tuff unit shown on the west half of the cross-section. VES 9 is approximately on the north projection of a probable north-trending splinter of the Hilton Creek fault upon which many of the hot springs are located. The altered tuff unit east of VES 9 may be faulted below detection of VES 13 and VES 14 and does not appear to be present beneath VES 26 and VES 28 or may never have been altered and therefore is included in the 45-100 ohm-meter material.

Cross-section B-B' is shown on plate 11. VES 8 is common to both profiles, B-B' and A-A'. The conductive part of the tuff unit must be constricted quite severely in a northerly direction because it does not appear on either VES 6 or VES 37 on either side of VES 8. Shown on plate 8 is the approximate limit of the conductive layer discussed above. The outline of the conductor shows that most of the total-field resistivity low centered about Cashbaugh Ranch must be caused mainly by this conductor. As mentioned previously, the fact that the resistivity low tends to extend westward onto outcrops of the altered tuff in the resurgent dome suggests that this is the unit causing much of the low, and the outline roughly determined by the sounding interpretations seems to bear out this conclusion.

One branch of the Cashbaugh low (pl. 4) extends from Whitmore Hot Springs northeast to the north end of Lake Crowley. Soundings in this

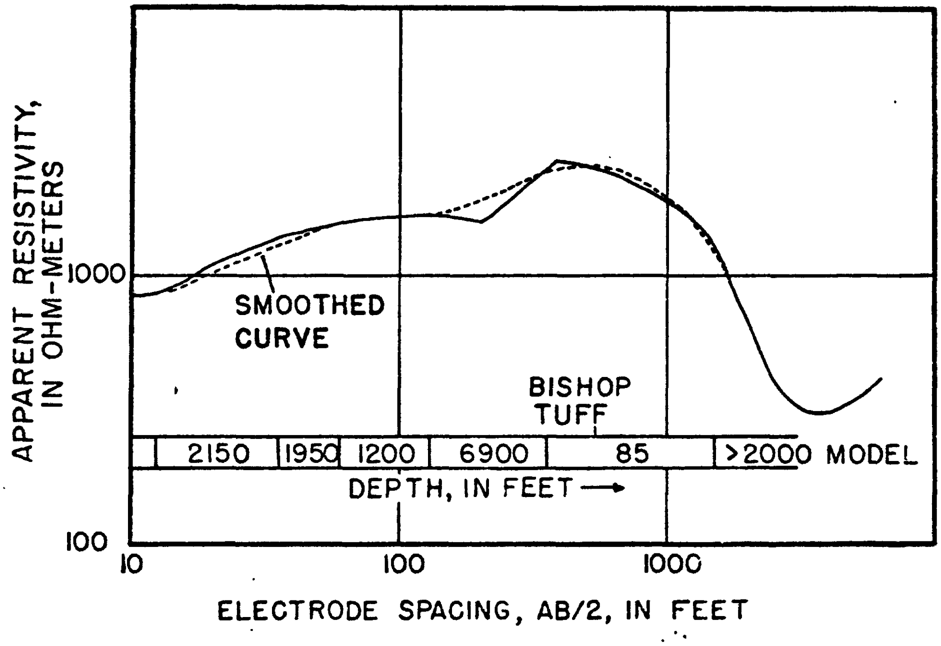

Figure 52.--Schlumberger sounding curve VES 35 on the Bishop Tuff. Numbers in bar-graph model represent interpreted true resistivities in ohm-meters.

vicinity (pl. 12) indicate that this low is caused by a conductor at depths greater than 500 m. The presence of this conductor is suggested on VES 2, VES 22, VES 24, VES 31, and VES 37 (pl. 13). On none of these soundings was the expression of the conductor fully developed, and its resistivity or thickness therefore could not be determined accurately. However, TMS 11 (near VES 31) and TMS 12 (near VES 2) provide some estimate of these parameters. The field data and model VES curves and models for the TMS data are shown on plate 13. Note that the TMS field data descend more steeply than the model curves for the late times (right-hand portions). For an infinite flat earth horizontally layered such that all the conducting layers on a particular TMS can be represented by a thin conductive sheet, the slope of the late-time portion of a transient curve plotted in logarithmic coordinates should eventually reach -5/2 (Jacobson, 1969, Vanyan, 1966). The greater negative late-time slope observed on the field data is probably an indication that the conductor is limited horizontally, which is also shown by the shape of the total-field low. The conductor is about 500 meters thick and has a resistivity of 5.4-12.5 ohm-meters. For this preliminary report the VES and TMS interpretations were not optimized for exact agreement between the two sets of data. For instance, the TMS 12 interpretation probably represents a minimum depth to the conductor, and the VES 2 interpretation represents a maximum depth to the conductor. These values are similar to those of the tuff unit discussed previously and may be representative of a similar unit, although the linear northeast trend of the total-field resistivity anomaly suggests that the conductor extent is largely fault related. VES 22 appears to be detecting a significantly deeper conductor, although the fact that VES 22 was expanded on the north end (see pl. 14) into the area of thickest near-surface conductive material (see VES 3) suggests it may be distorted.

The other major anomaly investigated with soundings is the electrical low near Casa Diablo. The locations of the soundings completed in this low are shown on plate 8. The smoothed sounding curves and interpretations are shown on figure 53. The <10 ohm-meter conductive layer shown

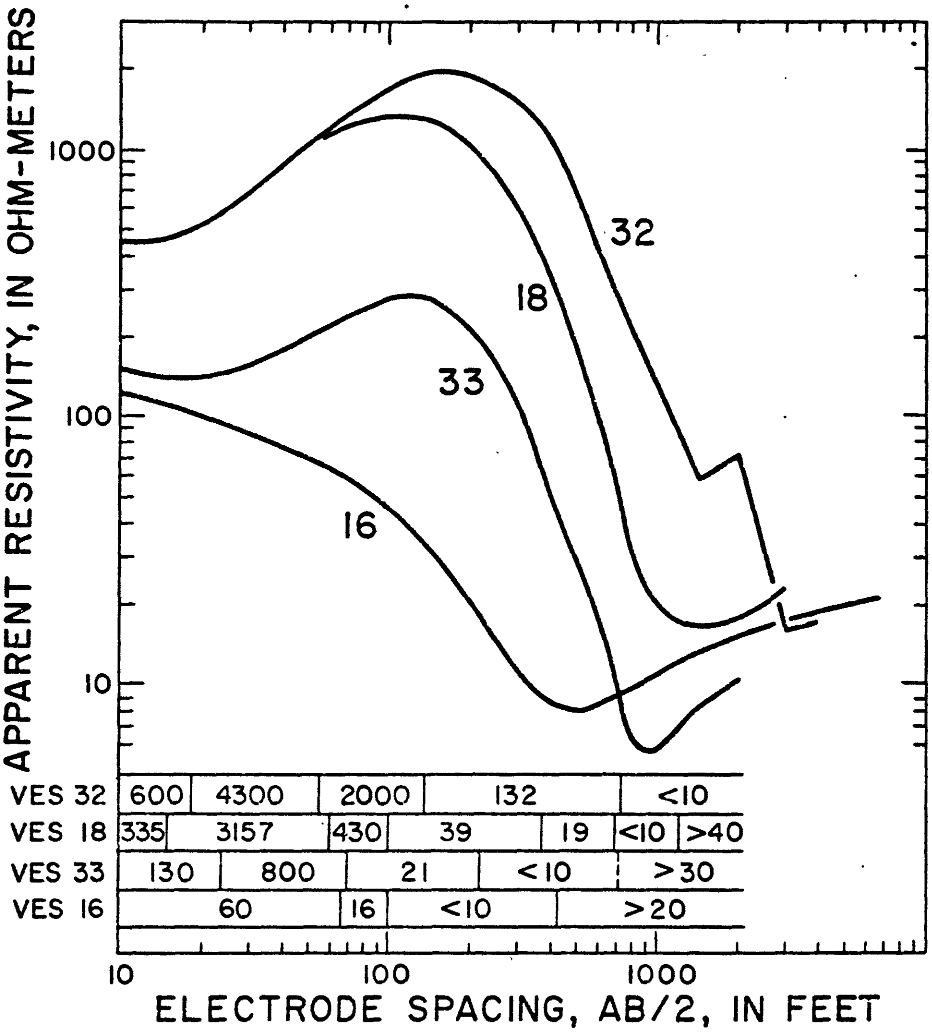

Figure 53.--Schlumberger sounding curves VES 16, VES 18, VES 32, and VES 33 with interpretations from near Casa Diablo Hot Springs. Numbers in bar-graph models are interpreted true resistivities in ohm-meters. Model interfaces are at depths scaled on AB/2 axis, in feet.

on the models is the cause of the resistivity low. This conductor is probably related to alteration caused by thermal waters rising along fracture zones. This relationship is suggested by the linear nature of the anomaly in an easterly direction, with a branch extending along the west side of the resurgent dome in a northerly direction. The Casa Diablo Hot Springs are believed to occur at the intersection of two sets of faults. One sounding, VES 19, confirms that a similar conductive zone may be the cause of the continuation of this low in a northerly direction along the west side of the resurgent dome. There is the suggestion of a similar low trending north from the Casa Diablo low on the aeromagnetic map, although the origins of these electrical and aeromagnetic lows may not be the same.

Conclusions

The geoelectrical data seem to support the interpretation that most of the thermal features in the Long Valley caldera owe their location to fault control of upward-moving thermal waters and that much of this faulting is directly related to regional Sierran fractures. The thermal water seems to have caused most alteration in a tuff unit occurring over a considerable portion of the caldera. The preliminary geophysical interpretations do not indicate any thick electrically conductive zones in the upper kilometer of Long Valley which contain water with temperatures much higher than those in test hole LV1 and surface springs. The main reservoir for thermal waters such as those issuing from the many hot springs must lie at depths greater than one kilometer. The direct-current and electromagnetic data do not give any conclusive indication of the possibility of this deeper reservoir with the exception that it may be expressed on VES 22, although this curve probably is distorted by lateral effects. The faults related to the Sierran front undoubtedly have fractured any deep reservoir and the best opportunities for obtaining significant commercial production of geothermal energy lie in the area of these major fractures as outlined by the resistivity maps.

References cited

Alpin, L. M., 1966, Dipole methods for measuring earth conductivity: New York, Plenum Press.

Anderson, W. L., 1973, Fortran IV programs for the determination of the transient tangential electric field and vertical magnetic field about a vertical magnetic dipole for an m-layer stratified earth by numerical integration and digital linear filtering: U.S. Geological Survey; available from U.S. Dept. Commerce, Natl. Tech. Inf. Service, Springfield, Va. 22151, as Rept. PB2-21240, 82 p.

Bailey, R. A., 1973, Post-subsidence volcanism and structure of Long Valley caldera, California: Geol. Soc. America Abs. with Programs, v. 5, no. 1, p. 7.

Jacobson, J. J., 1969, Deep electromagnetic sounding technique: Colorado School Mines Ph. D. thesis.

Keller, G. V., 1966, Dipole method for deep resistivity studies: Geophysics, v. 31, p. 1088-1104.

Keller, G. V., and Frischknecht, F. C., 1966, Electrical methods in geophysical prospecting: Oxford, Pergamon Press.

Pakiser, L. C., Kane, M. F., and Jackson, W. H., 1964, Structural geology and volcanism of Owens Valley regions, California--a geophysical study: U.S. Geol. Survey Prof. Paper 438.

Rinehart, C. D., and Ross, D. C., 1964, Geology and mineral deposits of the Mount Morrison quadrangle, Sierra Nevada, California: U.S. Geol. Survey Prof. Paper 385.

Vanyan, L. L., 1966, Electromagnetic depth soundings: New York, Consultants Bur. Translation by G. V. Keller.

Zohdy, A. A. R., 1973a, Automatic interpretation of resistivity sounding curves using modified Dar Zarrouk functions [abs.]: Geophysics, v. 38, p. 196-197.

______1973b, Total-field resistivity mapping: Soc. Explor. Geophysicists, 42d Ann. Mtg.

______197_, Use of Dar Zarrouk curves in the interpretation of VES data: U.S. Geol. Survey Bull. 1313-D (in press).